**Alma Mater Studiorum - Università di Bologna**

SCUOLA DI SCIENZE

Dipartimento di Chimica Industriale "Toso Montanari"

Corso di Laurea Magistrale in

# Chimica Industriale

Classe LM-71 - Scienze e Tecnologie della Chimica Industriale

# Synthesis of carbazole-based scaffolds for self-assembled Pd(II)-cages with TADF properties

Tesi di laurea sperimentale

**CANDIDATO**

Antonella Pizzolante

**RELATORE**

**Prof.** Stefano Stagni

**CORRELATORE**

**Prof.** Eli Zysman-Colman

**Ph.D.** Diego Rota Martir

**Anno Accademico 2015-2016**

ABSTRACT

This work was aimed to the preparation of new carbazole-type scaffolds decorated with donor and acceptor (D-A) substituents to be employed for the production of the corresponding Pd(II)-based cages. The design of the new molecules was essentially focused to the evaluation of their Thermally Activated Delayed Fluorescence (TADF) properties. A bottom-up method involving the stepwise functionalization – through aromatic nucleophilic substitution ($S_NAr$) followed by Suzuki coupling - of the starting 3,6-dibromo-9H-carbazole was developed. Once the desired organic compounds were obtained, their complexation with Pd(II) was performed in order to prepare the corresponding metalla-cages. All of the desired products showed optoelectronic properties. Absorption and emission spectroscopy was used to evaluate the electroluminescence properties and to characterize the different compounds. Moreover, PLQY and lifetime decays values were also included into the final work in accordance to the estimation of TADF characteristics studies.

Questo lavoro sperimentale ha come scopo la preparazione di un nuovo tipo di gabbie supramolecolari a base di palladio(II) tramite l'uso di leganti derivanti da nuovi composti organici caratterizzati da proprietà TADF (Thermally Activated Delayed Fluorescence). In primo luogo, è stata delineata una strategia sintetica in modo da realizzare leganti in grado di fornire un'emissione di tipo TADF. A tale scopo, la struttura dei leganti sintetizzati è caratterizzata dalla presenza di due unità con carattere elettron-donatore (carbazolo) e elettro-attrattore (benzofenone) sulla stessa molecola in modo da osservare transizioni di carica intramolecolari. Entrambi i leganti e i rispettivi complessi con il palladio hanno dimostrato avere proprietà luminescenti. Sono state, a tal proposito, utilizzate tecniche di spettroscopia di assorbimento e emissione per caratterizzare i composti desiderati. Inoltre, sono stati inclusi nel lavoro degli studi riguardanti i valori di resa quantica di luminescenza e i tempi di decadimento delle emissioni dei composti stessi in modo da poterne valutare le proprietà optoelettroniche e quindi verificare la presenza di un decadimento radiativo di tipo TADF.

# Index

1. INTRODUCTION ..... 4
1.2 Third-generation organic electroluminescence materials ..... 6
1.2.1 TADF photophysics ..... 7
1.2.2 Spin-Orbit Coupling ..... 9
1.2.3 Energy Singlet-Triplet States Gap ($\Delta E_{ST}$) ..... 10
1.3 Photophysics ..... 12
1.4 OLED TADF-emitting device ..... 16
1.5 Self-Assembly cages ..... 19
2 RESULTS AND DISCUSSION ..... 22
2.1 Objectives ..... 22
2.2 Synthesis of 3,6-dibromo-9H-carbazole ..... 24
2.3 First Synthetic Route: Suzuki reaction ..... 25
2.4 Second Synthetic Route: ..... 26
Functionalization of the –NH of 3,6-dibromo-9H-carbazole ..... 26
2.4.1 Ullman reaction towards –NH of 3,6-dibromo-9H-carbazole ..... 28
2.4.2 Aromatic nucleophile substitutions ..... 29
2.4.3 Synthesis of 9-(4-nitrophenyl)-3,6-dibromo-carbazole ..... 30
2.4.4 Synthesis of (4-(3,6-dibromo-9H-carbazol-9-yl)phenyl)(phenyl)methanone ..... 30
2.4.4 Suzuki reaction on 4-(3,6-dibromo-9H-carbazol-9-yl)phenyl)(phenyl)methanone ..... 32
2.4.5 Suzuki reaction on 4-(3,6-dibromo-9H-carbazol-9-yl)phenyl)(phenyl)methanone ..... 34
2.5 Synthesis of supramolecular cage with $Pd^{2+}$ and ..... 35
(4- and (3-(3,6-di(pyridin-4-yl)-9H-carbazol-9-yl)phenyl)(phenyl)methanone ..... 35
2.5.1 Supramolecular complexation of Pd(II) towards 4-pyridyne ligand. ..... 38
2.5.2 Supramolecular complexation of Pd(II) towards 3-pyridine ligand ..... 41
2.6 Photophysical Properties ..... 42
2.6.1 AP013 and AP021 Absorption Spectroscopy ..... 43
2.6.2 AP019 and AP022 Absorption Spectroscopy ..... 44
2.6.3 AP013 and AP021 Steady State Emission properties ..... 45
2.6.4 AP019 and AP022 steady state emission spectra ..... 47
2.7 Solid state emission properties ..... 49
2.8 Energy gap ($\Delta E_{HOMO/LUMO}$) ..... 51
2.8.1 DFT calculation ..... 51
2.8.2 Cyclic Voltammetry ..... 53
3 Conclusive remarks ..... 56

4 Experimental Part ..... 57
4.1 General Synthetic Procedures ..... 57
4.2 Photophysical data ..... 58
4.3 Synthesis of 3,6-dibromo-9H-carbazole ..... 59
4.4 Synthesis of (4-(3,6-dibromo-9H-carbazol-9-yl)phenyl)(phenyl)methanone ..... 60
4.5 Synthesis of ..... 61
(4-(3,6-di(pyridin-4-yl)-9H-carbazol-9-yl)phenyl)(phenyl)methanone ..... 61
4.6 Synthesis of ..... 62
(4-(3,6-di(pyridin-3-yl)-9H-carbazol-9-yl)phenyl)(phenyl)methanone ..... 62
4.7 Synthesis of 3,6-dibromo-9-phenyl-9H-carbazole ..... 63
4.8 Synthesis of supramolecular cage with $Pd^{2+}$ and ..... 64
(4-(3,6-di(pyridin-4-yl)-9H-carbazol-9-yl)phenyl)(phenyl)methanone ..... 64
4.9 Synthesis of supramolecular cage with $Pd^{2+}$ and ..... 65
(4-(3,6-di(pyridin-3-yl)-9H-carbazol-9-yl)phenyl)(phenyl)methanone ..... 65
Bibliography ..... 66

This project was developed at the University of Saint Andrews, Scotland, in the laboratories of Eli Zysman-Colman. Members of the Zysman-Colman group conduct research at the interface of organometallic, optoelectronic materials, physical organic, and supramolecular chemistry. They use a combination of organic synthesis, coordination chemistry, varied analytical techniques such as NMR, mass spectrometry, fluorimetry, and cyclic voltammetry, coupled with molecular modeling to address research goals relating to electroluminescence.

# 1. INTRODUCTION

The concept of organic semiconductors was established in the 50s and 60s. In 1965 Helfrich and Schneider observed the organic electroluminescence from an organic compound, anthracene single crystal, for the first time. [1]

The challenge in synthesizing novel semiconductor organic compounds led to the development of Organic Light-Emitting Diodes (OLEDs). Gradually the research on OLEDs focused on ultrathin films rather than single crystals to realize low-voltage operations. OLEDs are mentioned in literature as the first devices based on organic thin films capable of being operated at current densities as low as $mA/cm^2$ order and are considered to be the core organic optoelectronic devices realized by utilizing organic compounds as semiconductor. Since 2000, the full-scale research and development of organic electronic devices was carried out from academic research and subsequently expanded into practical applications, including small-medium-sized mobile devices, artificial lighting and TV Screens.[1]

Although OLEDs are characterized by high flexibility, resolution and EL efficiency, their performance can still be improved avoiding the use of very expensive noble metals in the emitting materials in order to create low cost fabrication process and achieving both high definition a stable blue emission, that are required for medium and small-sized OLEDs.

The result of these new challenges is a wide range of fluorescent and phosphorescence materials that can be distinguished chronologically in three different generations. The first generation includes fluorescent materials that have been mostly applied for durable OLEDs devices although the internal quantum efficiency, which is defined as the ratio of the number of photons that can be extracted for EL to the injected current, was only 25% because of the  the limit of harvesting only the fluorescent excitons.

In the late 90s the second generation of devices involving phosphorescent materials, has taken hold achieving an internal quantum efficiency of 100% due to the contribution of the triplet state (75%) to luminescence. In contrast to fluorescent materials, the design of phosphorescent molecules is limited because the heavy atom effect (spin-orbital interaction) must be induced by using second and, in particular, third row transition metals, to realize highly efficient radiative processes from the triplet excited state to the ground state.[1]

The discovery of a new method of developing phosphorescent materials that are free of rare metals and which generates a singlet excited state by triplet-triplet annihilation (TTA) was the crucial point which led to the next generation of devices. In 1960s scientists observing the anthracene single crystals already recognized the TTA as a delayed fluorescence phenomenon. The TTA deactivates the triplet exciton, thus the EQE decreases for phosphorescent light emitting materials and increases the concentration of singlet excitons. On the other hand, TTA can be used to increase the singlet

excitons in fluorescent materials and to improve the EQ efficiency. However, only 37.5% of singlet excitons can be generated by TTA delayed fluorescence.[2]

Recently a new strategy has been developed in order to achieve 100% of singlet generated excitons, it is called E-type Delayed fluorescence and it consists of the up-conversion from triplet excitons (75%) upon electrical excitation to singlet excited state by thermal energy activation. Therefore the third generation includes all the materials that exhibit thermally activated delayed fluorescence (TADF), whose characteristic will be explained in the following paragraphs. [3]

TADF technologies gave rise to a new category of luminescent materials, contributing to the academic progress in field. The attractiveness of organic compounds lies in the diversities of molecular structures, and TADF materials are considered as novel materials created by making full use of that diversity. The TADF phenomenon has been profoundly examined since 2010, in particular by Adachi and his group of the Center for Organic Photonics and Electronic Research at Kyushu University. TADF technologies add new and promising development in the panorama of OLEDs. A further generation of TADF is called Hyperfluorescence, which is characterized by highly efficient blue emission from both singlet and triplet states reaching an EQE of 100%. The great cost savings of Hyperfluorescence materials together with their high luminescent efficiency contributes to the actual state of art of the novel OLEDs' market.[4]

In the last few years, a combination of supramolecular chemistry and photochemistry has led to design and construction of supramolecular systems capable of performing interesting light induced functions. Photoinduced energy and electron transfer are indeed basic process for connecting light energy inputs with optical, electrical and mechanical functions. This branch of studies leads to a new range of metallo supramolecular structures as components of functional nanodevices. In particular, Fujita's research group focused on the synthesis of photoinduced electron transfer between encapsulated guest molecules and metallo supramolecular host, resulting in structures capable of redox reduction and catalytic process.[5,6]

In this work it has been examined a new synthetic route for a novel organic bispyridyl-carbazole based emitter molecule with TADF properties. The design of the molecule was carefully carried out according to literature.[7] The core of the work is to find a way to synthetize an organic compound with the "right" geometrical and structural requirements for obtaining self assembled Pd(II)-based supramolecular systems with efficient emission properties.[8]

## *1.2 Third-generation organic electroluminescence materials*

TADF represents the third generation of electroluminescent organic materials, it overcomes the previous generation in terms of electroluminescence efficiency, technological properties and effective costs of production. As far as we use fluorescence, as in tris(8-quinolinolato)aluminum(III) characterized by an emission which comes from $^{1}\pi$-$\pi^{*}$ transition, the exciton efficiency is limited to 25% and the excited state lifetime is estimated to be around 15 ns, which is a quite short lifetime. The advantages of using fluorescent materials are that there is no limit to their molecular design and their low production costs.

Phosphorescent materials have been considered for long time the only solution to gain 100%EQE thanks to the harvesting of the triplet state. Among them the typical choices are either Iridium complexes as $Ir(ppy)_3$ ,whose emission comes from a metal ligand charge transfer $^{3}$MLCT, Pt-OEP characterized by a triplet state $^{3}\pi$-$\pi^{*}$ emission of the ligand or $Eu(tta)_3$phen. In the last compound the optical excitation is absorbed by the ligand with the formation a singlet state, then the inter system crossing to the triplet state allows the emission from f-f transitions. In this case, the excited annihilation process is strong in fact the excited state lifetime of phosphorescent molecules is estimated around the orders of milliseconds. However, the design of phosphorescent new molecules is limited and the cost very expensive.[9]

However, despite their displaying fluorescent emission, substrates such as eosins, fullerenes and porphyrin derivatives are materials that exhibit thermally activated delayed fluorescence. TADF is a new way to harvest electronically generated excitons that strongly depends on the reverse intersystem crossing (RISC) from triplet to singlet excited states.[4]

*1.2.1 TADF photophysics*

Two distinct unimolecular mechanisms exist for molecular fluorescence: prompt fluorescence (PF) and thermally activated delayed fluorescence (TADF). In the PF mechanism, emission occurs after $S_n \leftarrow S_0$ absorption and excited state relaxation to $S_1$. The TADF mechanism takes place via the triplet manifold: after excitation and once attained $S_1$, intersystem crossing (ISC) to the triplet manifold $T_1$ or a higher triplet state occurs, followed by a second ISC from $T_1$ back to $S_1$, and by fluorescence emission.[10]

The energy diagram of a conventional organic molecule is represented in Figure 1a; the triplet excited state $T_1$ is lower than the singlet excited state $S_1$ in energy by 0.5-1 eV because of the electron exchange energy between these levels. However, the careful design of organic molecules can lead to a smaller energy gap between S1 and T1 excited states as shown in Figure 1b, which enhances the ISC between these states. Such excited states are attainable by intramolecular charge transfer within systems containing spatially separated donor and acceptor moieties.[11]

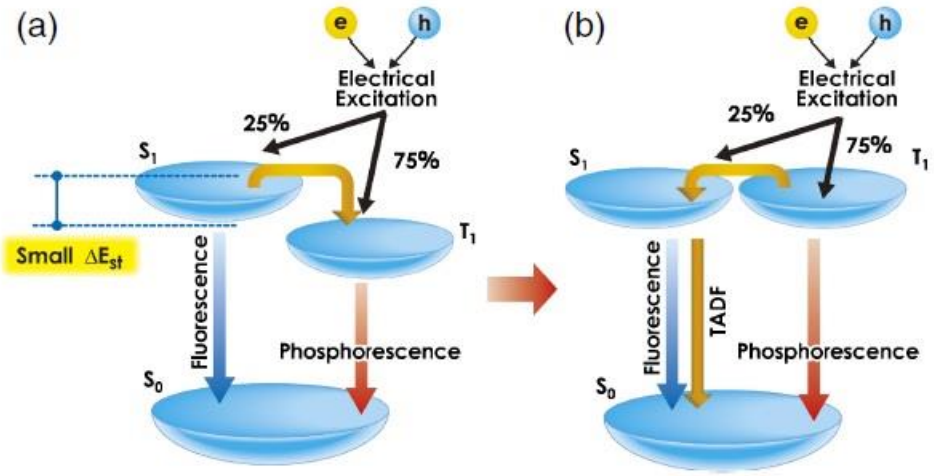


*Figure 1 a) conventional fluorescent and phosphorescent materials. b) For TADF materials, the $S_1$ and $T_1$ levels are close to each other and RISC occurs with high efficiency.* [10]

The simplest model for thermally activated delayed can be represented by the following kinetic scheme (Scheme 1):

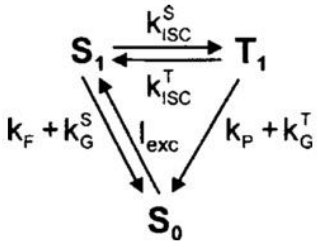


*Scheme 1 Kinetic scheme of TADF.*

where $I_{exc}(t)$ is the excitation intensity, $k_F$ and $k_P$ are the radiative rate constants for fluorescence and phosphorescence, respectively, $k_G^S$ and $k_G^T$ are the nonradiative rate constants for deactivation to the ground state (internal conversion from $S_1$ and intersystem crossing from $T_1$, respectively), and $k_{ISC}^S$ and $k_{ISC}^T$ are the ISC rate constants for singlet-to-triplet and triplet-to-singlet conversions, respectively.

For strong TADF to occur $k_{ISC}^S >> k_F + k_G^S$ and $k_{ISC}^T >> k_P + k_G^T$, in most cases $k_{ISC}^S >> k_{ISC}^T$ and $k_G^T >> k_P$.

TADF is significant only when the quantum yield of triplet formation $\phi_T$ and the quantum yield of singlet formation $\phi_F$ are both high.

$$\phi_T = \frac{k_{ISC}^S}{k_F + k_G^S + k_{ISC}^S}$$

$$\phi_S = \frac{k_{ISC}^T}{k_P + k_G^T + k_{ISC}^T}$$

This in turn implies a small energy gap between $S_1$ and $T_1$, a long $T_1$ lifetime.[10]

*1.2.2 Spin-Orbit Coupling*

Once the triplet state is formed, excited species can decay either radiatively, promoting emission of light or non-radiatively. In this case, a possible decay is the reverse intersystem crossing (RISC) from triplet to singlet which is allowed by spin-orbit coupling. Generally, heavy metals promote spin conversion and provide the spin-orbit coupling which is required for ISC and RISC. Organic compounds have not this intrinsic property so it has to be induced by new molecular design according to the following Equation 1

(Equation 1) $$\lambda = \frac{Hso}{\Delta E_{ST}}$$

The first-order mixing coefficient between singlet and triplet states (λ) is correlated to the energy gap between singlet and triplet states ($\Delta E_{ST}$) and the spin-orbit interaction ($H_{SO}$).

The spin orbit Hamiltonian in Equation 2 represents the coupling between the spin and orbital momenta of an electron *i* through interaction with the nucleus where α is the fine structure constant, $Z_\mu$ is the effective nuclear charge and L and S are the orbital and spin momenta. Electron-electron interactions have been neglected to simplify the Hamiltonian although those interactions should be included for the description of spin-orbit interactions.[12]

(Equation 2) $$Hso = \alpha \sum_{\mu}^{N} \sum_{i}^{n} \frac{Z_\mu}{r_{i\mu}^3} L_i S_i$$

Efficient spin conversion can be achieved with molecules with a small $\Delta E_{ST}$ whether the value of $H_{SO}$ is not approaching zero. Therefore the aim is to synthesize organic molecules with a small band gap in order to have ISC and RISC (higher λ values). The probability of RISC increases as the energy gap between singlet and triplet states decreases ($\Delta E_{ST}$), for example keto-based materials have an enough small gap of 0.1-0.2 eV to exhibit TADF properties.[13]

*1.2.3 Energy Singlet-Triplet States Gap ($\Delta E_{ST}$)*

Quantum chemistry can explain how to reduce the $\Delta E_{ST}$ which is proportional to exchange energy (K, Equation 3) between two electrons,

(Equation 3) $$K = const * \langle \pi(r_1)\pi^*(r_2) \left|\frac{1}{r_{12}}\right| \pi(r_2)\pi^*(r_1) \rangle$$

$\pi$ and $\pi^*$ are the HOMO and LUMO functions, $r_1$ and $r_2$ are the spatial coordinates and $r_{12}$ is the electron-electron separation distance.[14]

In the Equation 3, the mentioned exchange energy is proportional to the overlap integral between the HOMO and LUMO orbital, so the energy band gap can be estimated depending on the overlap of the orbitals. On the other hand, the $\Delta E_{ST}$ is inversely proportional to its spatial separation (Figure 2). According to this, when nonbonding orbital and the excited π-electron orbital overlap orthogonally, as in benzophenone molecules, $\Delta E_{ST}$ decreases as a consequence of the small overlap. Contrary, a large $\Delta E_{ST}$ comes from a large overlap π-π* orbital which is typical of aromatic compound, thus spin orbit interactions between π-π* is expected to be very weak.[12]

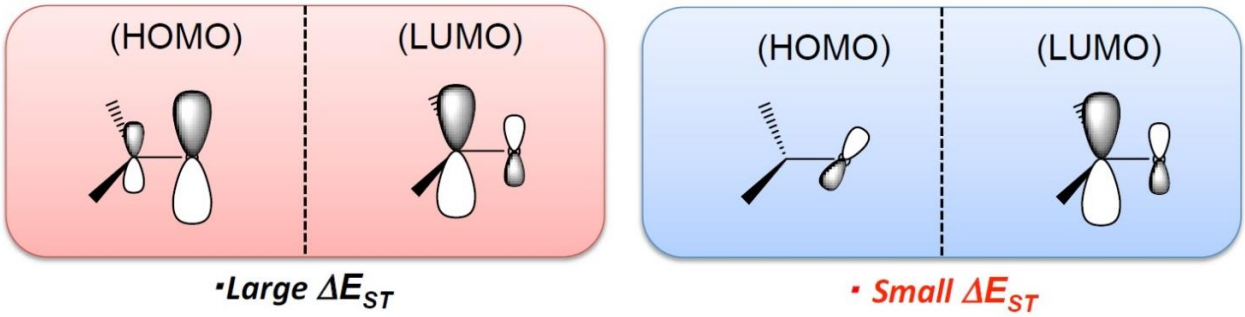


*Figure 2 Representation of HOMO/LUMO orbitals in correlation with the $\Delta E_{ST}$*

The triplet excited state $T_1$ is described, in terms of a few electronic configuration, with a strong π character so the electronic excitations should have a sigma character rather than a π-π* one in order to have a large spin orbital coupling. This is achieved with a very small gap between the singlet and triplet excited states. According to the huge range of compounds reported in literature, there are different ways of achieving spin orbit coupling depending on the nature of molecules and varying some characteristics during their synthesis. For example many heterocyclic compounds have been exploited as long chain oligothiophenes, it has been observed that the raising of twist angle between adjacent rings increase the spin orbit coupling whereas the increasing of chain length reduces the σ-π mixing and hence the spin orbit interactions. Moreover, the spin orbit coupling depends on the atomic number Z so adding heavy-atom-containing groups as chlorine and bromine induces its enhancement.[12]

An effective way to synthetize novel TADF molecules is to focus on the introduction of electron-accepting and electro-donating units into one molecule to realize molecules with small $\Delta E_{ST}$, moreover the RISC is enhanced by intramolecular charges transfer in systems with separated acceptor and donor moieties. The accepting unit localizes the LUMO orbital whereas the donating unit localizes the HOMO orbital. However, the critical point of this design is the conflicting combination of a small $\Delta E_{ST}$ and a needed radiative decay of $10^{-6}$ $s^{-1}$ to achieve an acceptable electroluminescence yield, in fact both limited orbital overlap and small $\Delta E_{ST}$ results in no emission. Since the radiative decay is proportional to the overlap integral between HOMO and LUMO, the solution is to maintain a small HOMO-LUMO overlap within the molecule.

## *1.3 Photophysics*

Following the absorption of a quantum of energy, a molecule is promoted from the ground state to the corresponding excited state(s). According to Boltzmann distribution, the majority of organic molecules are at the ground state at room temperature because electrons have not enough energy to reach any excited states.

First of all, organic molecules mostly have a closed-shell ground-electronic configuration, and therefore the ground state is a singlet state, usually indicated with $S_0$. When an electron is promoted from one of the low-energy occupied MOs to a high-energy unoccupied orbital, singlet, and triplet states occur in pairs. Each triplet state is lower in energy than the corresponding singlet, because of spin correlation, and has a different multiplicity from that of the ground state.

Once the energy is absorbed, the molecule changes from the ground state to a vibrational and rotational excited electronic state $S_1$. This excited state is unstable and the molecule undergoes spontaneously either radiative decays, that employ the emission of photons, or non-radiative decays, represented into the Jablonsky diagram (Figure 3).

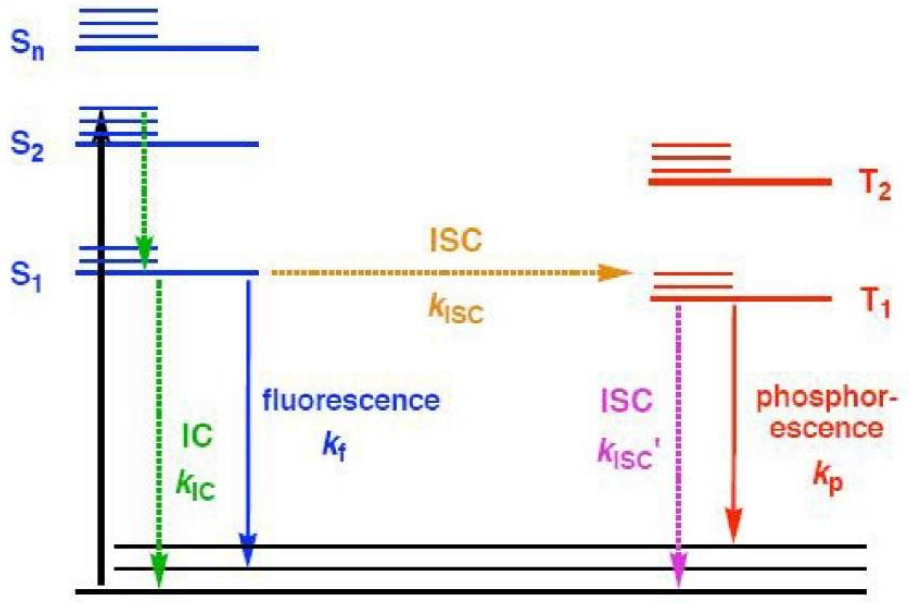


*Figure 3 Diagram of Jablonsky*

Vibrational relaxation, Internal Conversion (IC) and Intersystem Crossing (ISC) are classified as non-radiative decays whose effect is to convert the light in thermal energy. Generally, excited molecules after absorption transfer their vibrational energy to other molecules including the solvent, *via* Vibrational Relaxation, with no emission of photons. The energy transfer from the excited state $S_1$ occurs through either IC transitions between states of equal multiplicity ($S_1 \rightarrow S_0$) or ISC transitions between states of different energies and different multiplicity($T_1 \rightarrow S_0$) followed then by vibrational relaxations (ISC'). These mentioned non-radiative decays take the excited molecules to lower vibrational energy states.

According to Kasha's rule, radiative processes (i.e. emission) occur only from the lowest excited state.

A molecule can emit a photon from both $S_1$ and $T_1$ state to reach the $S_0$ state, in this case the phenomenon is well-known as luminescence. If the decay involves transitions between excited and ground states with same multiplicity ($S_1 \rightarrow S_0$) fluorescence is observed, while the phosphorescence originates from excited states with multiplicity different ($T_1 \rightarrow S_0$) than the one that characterizes the ground state.

Fluorescence and phosphorescence are both very rare in organic molecules and depend not only on the molecule itself but also on solvent and physical properties as pressure and temperature. Moreover, intersystem crossing processes are strictly related to phosphorescence, it means that $T_1 \rightarrow S_1$ transitions can occur before $T_1 \rightarrow S_0$ emissions lowering the rate of emission from the triplet state. Thus fluorescence is a fast process, whose lifetimes values are included in a range of $10^{-8}$-$10^{-2}$ s with no change in multiplicity whereas phosphorescence is a slow process. Because of the change in multiplicity, phosphorescence's life times are longer ($10^{-4}$-$10^{2}$ s).[15] The destiny of the decays are confined into kinetic field,

$$\tau = \frac{1}{k_{rad} + \sum k_{nr}}$$

relying on the rate constant of radiative decays $k_{rad}$ and non-radiative deactivation pathways $\sum k_{nr}$.

Usually in organic conjugated compounds fluorescence radiative rate decay $k_f$ is around $10^8$ $s^{-1}$, if the value is comparable to $\sum k_{nr}$ fluorescence is observed. On the other hand, phosphorescence is rare because $k_p$ is much smaller than $k'_{ISC}$, it might be observed if $k_{ISC} >> k_f + k_{IC}$ that is usually induced by Spin-Orbit coupling.

An effective way to quantify the efficiency of emissions is to evaluate the quantum yield (emitted photons/absorbed photons) of both fluorescence $\phi_f$ and phosphorescence $\phi_p$,

$$\phi_f = \frac{k_f}{k_f + k_{IC} + k_{ISC}}$$

$$\phi_p = \frac{K_{ISC}}{k_f + k_{IC} + k_{ISC}} \cdot \frac{k_p}{k'_{ISC} + k_p}$$

this parameter is noteworthy used to distinguish the nature of radiative decays by quenching the triplet state. Triplet dioxygen ($^3O_2$) is a quencher of triplet states, and the probability of oxygen quenching increases along with the lifetime of the triplet state itself. Quantum yields of degassed and aerated (air equilibrated) solutions, respectively $\phi_{deg}$ and$\phi_{aer}$ are correlated to the solution Oxygen concentration through Stern-Volmer quenching constant $K_Q\tau$

$$\frac{\phi_{deg}}{\phi_{aer}} = 1 + K_Q\ \tau[O_2].$$

Quantum yields of phosphorescent degassed solution samples are higher than degassed ones whereas there should not be significant changes in fluorescent solutions between degassed and aerated samples.

Luminescence strongly depends on the distortion of excited states compared to ground states. Depending on the difference in the equilibrium geometry of the ground and excited states, the excitation could cause either change in size or shape of complexes. In general, a good "rule of thumb" for the obtainment of luminescent molecules is the use of rigid scaffolds. In such case, the molecule in the excited state is slightly distorted with respect to the same species considered at the ground state. This prevents or minimizes the occurrence of non-radiative decays (b) through vibrational relaxations (pathways). Respectively, good emissions can be obtained with rigid scaffolds or ligands, in contrast rates of IC and ISC from excited states to ground states are promoted by large differences in geometry

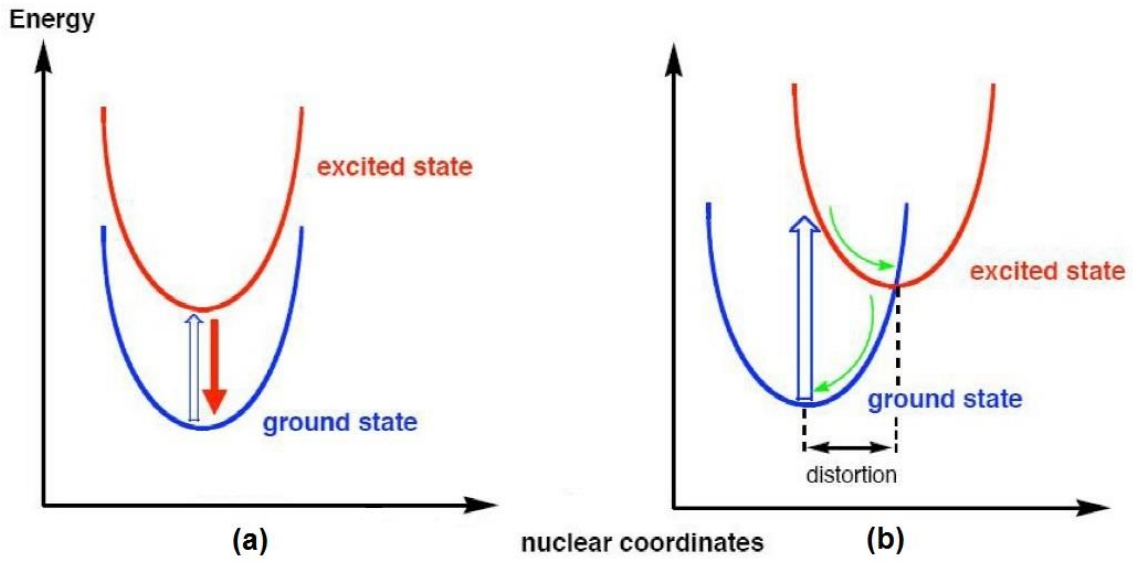


*Figure 4. Schematic representation of the relation between bandwidth and equilibrium nuclear configuration in the ground and excited state.*

Furthermore, it is essential to prevent distortion for molecular compounds in solution. In inorganic metal complexes d-d transitions lead to a significant distortion of the geometry of the resulting excited state in comparison to that of the complex at the ground state. This effect is very important in the cases of the first row transition metal complexes, where the population of lowest excited state originates from a d-d (Metal Centered, MC) transitions. On moving to transition metals belonging to second and third row, d-d states are raised at higher energy, making them less accessible in favour of the population of less distorted states arising from Metal to Ligand Charge Transfer (MLCT) and, eventually, Ligand Centred (LC) –type transitions. Also, the introduction of second and third row transition metals leads to the increase of spin-orbit coupling effect, which leads to a more efficient ISC and, consequently, to the occurrence of phosphorescent T→S transitions.[16].

Due to the lack of a heavy atom such as transition metals, the population of excited states with triplet multiplicity in organic molecules is a very difficult task and the design concepts leading to phosphorescent organic molecules and, in particular, to those capable of Thermally Activated Delayed Fluorescence (TADF) are described further on. In general, two different strategies are promising to control and limit excited distortion during the design and application of TADF materials. The first approach is to optimize the matrix material used in TADF devices to avoid excited state distortion of the doped material. The second one, is based on modifying the chemical structure of the compound so that the geometry distortions upon excitation are reduced by sterical interactions of the ligands in case of metal-based TADF or by bulky groups for organic TADF molecule.[17]

## *1.4 OLED TADF-emitting device*

An organic light-emitting diode (OLED) is a light-emitting diode (LED) in which the emissive electroluminescent layer is a film of organic compound that emits light in response to an electric current. In multilayered OLED devices, indium tin oxide (ITO) is used as a transparent anode electrode and an evaporated metal is used as a cathode. Layers of organic compounds capable of carrying charges and light emitting are deposited on the transparent substrate by spin coating or high vacuum sublimation. An n-doped electron injection layer or a metal layer is used to inject electrons, these layers are unstable in air and need encapsulation.

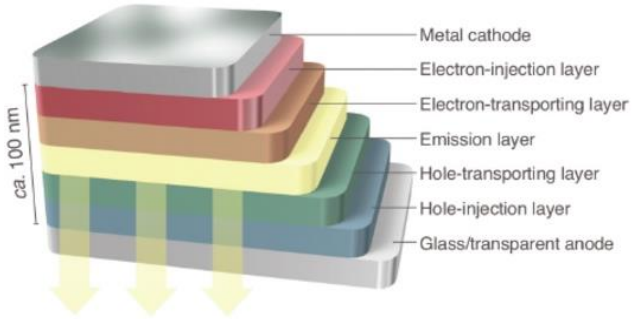


*Figure 5 Device architecture of typical OLEDs.*

The working principle of an OLED is based on four steps (Figure 6). At first, a proper bias is applied with the injection of electrons and holes, then the charges move through the molecules to the other electrode in the presence of the applied electric field (2a, 2b). The recombination of electrons and holes led to the formation of an exciton (4), a molecular excited state that can deactivate radiatively to generate a photon.[18]

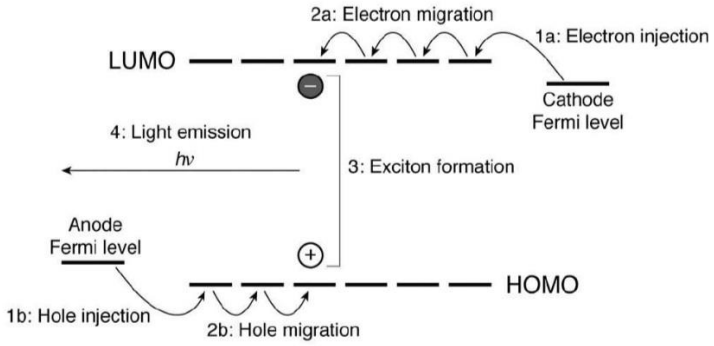


*Figure 6 The working principle of an OLED is based on four steps.[17]*

The color of the emitted light depends on the energy of emitting excited state. The most used materials are metal complexes characterized by efficient phosphorescence as cyclometalated $Ir^{III}$

complexes. However, these phosphorescent materials suffer for instability in practical applications, especially for blue and white emission.[3]

Species capable of TAD fluorescence have been exploited since organic molecules displaying high phosphorescence at the solid state are very rare. The challenge is to rationally design novel families of TADF luminophores based on simple versatile molecular scaffolds that exhibit emission across the entire visible range. The research focused both on the synthesis of new emitting layers and new host materials for these emitting dopant. The dopant-host interaction is also crucial to obtain high quantum efficiency, in fact the host material should have higher $S_1$ and $T_1$ energy levels than those of the emissive dopant, efficient energy transfer to the dopant, low carrier injection barriers from both the carrier's layers and efficient exciton confinement.[19]

The process of population of an excited state of the emitter complex proceeds via singlet ($^1$CT) and triplet ($^3$CT) charge transfer states. ISC time is longer than relaxation times to lower lying states with the same multiplicity (IC), because of the very small splitting between these two states and the small SOC of the host material, the host material has to be designed in order to have an ISC from the $S_1$ to the $T_1$ state.[20]

The benchmark of OLED TADF-emitting device performance is around 20% EQE using small donor-acceptor-donor (D-A-D) molecules that create an intramolecular charge transfer (ICT) state between the electron donating and accepting moieties.[9,21]

Recently, Cu(I) multi-bridged dinuclear complexes opened the door to very efficient OLEDs because of their low cost production and relatively straight forward synthesis. These complexes exhibit certain key properties allowing to harvest all excitons, singlet and triplet states, that are generated in the emission layers for the generation of light. The best EQE obtained for this class of compound is around 23%.[17]

An effective way to synthetize novel TADF molecules is to focus on the introduction of electron-accepting and electro-donating units into one molecule to realize molecules with small $\Delta E_{ST}$, moreover the RISC is enhanced by intramolecular charges transfer in systems with separated acceptor and donor moieties. The accepting unit localizes the LUMO orbital whereas the donating unit localizes the HOMO orbital, moreover bulky groups can be introduced in order to enhance the localization. However, the critical point of this design is the conflicting combination of a small $\Delta E_{ST}$ and a needed radiative decay of $10^{-6}$ $s^{-1}$ to achieve an acceptable electroluminescence yield, in fact both limited orbital overlap and small $\Delta E_{ST}$ results in no emission. Since the radiative decay is proportional to the overlap integral between HOMO and LUMO, the solution is to maintain a small HOMO-LUMO overlap within the molecule.

## *1.5 Self-Assembly cages*

The self-assembly of giant polyhedral complexes from metal ions and bridging ligands attracts considerable interest because it provides an efficient bottom-up approach to afford well-defined nanoscale structures. Although these species exhibit molecular recognition, catalytic and biological properties they are not yet widespread because of their tricky synthesis and characterization.[22]

More recently, a range of photophysically interesting architectures have been synthesized and examined. These have included systems that incorporate photophysically active metal ions as structural units within the architecture framework, as well as those that employ luminescent organic spacer units within the ligand scaffold. These species offer the potential for a new generation of molecular sensors and photocatalysts, among others.

The science's challenge is to find out a way to obtain photophysically active metallo-supra- molecular systems in which the coordination of the metal ions to the ligands does not result in inhibition of the desired functionality. In fact, it is difficult to maintain the properties of either the metal or the ligand if assembled in a complex structure. Moreover, it is difficult to find a compromise between the molecular structures that an organic compound should have to be either a good emissive molecule or a great and efficient ligand able to coordinate the metal core.[8]

Many of the metal ions that display desirable photophysical properties are second- or third-row transition metals, which are quite kinetically inert. This may result in low yields of the desired assembly due to kinetically inert metal centers impeding formation of thermodynamically favored products. Some works reports that exo-functionalization of the ligand system is a successful way to retain the self-assembly ability for the formation of a certain cage.

Fujita and co-workers reported the formation of different systems very sensitive to the geometry of the ligand used. Especially, his research focused on the self-assembly of the giant 5-nm diameter $M_{24}L_{48}$ spherical framework from $Pd^{2+}$ square planar ions and bent dipyridylthiophene ligands. Varying the ligand angle mixing bispyridal ligands as 1 (149°) and 3 (127°) (Figure 7) revealed that a slight change of the mean ligand angle can switches the final structure between $M_{24}L_{48}$ and $M_{12}L_{24}$, respectively 2 and 4 in the Figure 7. [7]

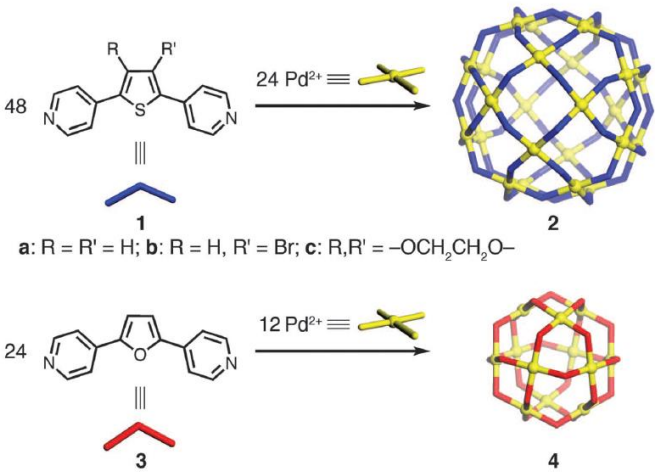


*Figure 7 Palladium cages: $M_{24}L_{48}$ (2) and $M_{12}L_{24}$ (4)*

Other pyridine based examples have been reported, as macrocyclic dinuclear complexes self-assembled starting from a source of (en)Pd $(NO_3)_2$ as metal core. The reaction of (en)Pd$(NO_3)_2$ and the pyridine based bridging ligand leds to different dimers or trimers depending on the angle of the ligand used. In this case, attachment of long and short lived states emitting ligand units are appended into the molecular framework without altering the properties of the emitter.[23] Anyway various compound featuring monodentate nitrogen-containing ligands have already been tested in TADF devices. In particular, bispyridil-tetrazoyl based Cu (I) complexes were estimated to be very interesting with a 15% EQE. These complexes revealed very good applications as powder or polymer doped material for delayed fluorescent devices. In spite of this, slightly changes of the ligand in these complexes completely changed the quantum yields of their emission. Thus, rigidity in required for both complexes and self-assembled cages that are designed and produced to act as emitter. [17]

In this work, we focused on the synthesis of a novel TADF material, the first step was indeed to project the design of the molecule with the desired properties. Thus it was investigated not only the synthetic route of the new molecule but also its optoelectronics properties *via* emission and absorption spectra.

However, we added another requirement during the synthetic design: to include two peripheral pyridine rings in order to obtain a new symmetric organic bispyridyl-carbazole based target as shown in Figure 8. It acts as bridging ligands towards the preparation of a supramolecular assembly based on coordination between the nitrogen of the distal pyridine units and $Pd^{2+}$ ions the metallic Palladium cations.[24,25]

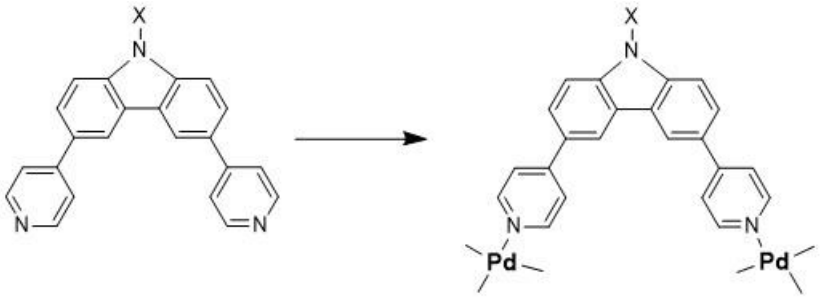


*Figure 8 Synthetic route to achieve supramolecular assembly towards Pd(II)*

According to various examples already reported in literature, we discussed the chance of making a novel self-assembled Palladium cage varying the ligand angle moving the Nitrogen site from position 3 to 4, of the outlying pyridines. Although identification of these supramolecular structures is very complex, the core of this study is to focus on the optical properties of the desired assemblies in solid and solution states in order to achieve delayed fluorescent emission from either the global framework or the ligand.

# 2 RESULTS AND DISCUSSION

## *2.1 Objectives*

Recently, phosphorescence organic light emitting diodes and Thermally Activated Delayed Fluorescence (TADF) OLEDs have attracted extensive attention, since they can reach a theoretical maximum internal quantum efficiency of 100% by utilizing both the singlet and triplet excitons for light emitting.

As far as the TADF materials might be potentially applied not only in OLEDs but also in metallo-supramolecular architectures, herein it will be investigated the chance of synthetizing a novel family of exo-functionalized metallo-supramolecular cage architectures constructed from pyridine backbones. The starting purpose is to synthetize a range of novel molecular donor acceptor (D-A) targets capable of displaying TADF properties both in solution and in solid state, in fact the doping-dedoping process leads to the required alteration of band gap.

According to the literature, TADF molecules should be designed in order to meet the following requirements:

- Small energy gap between $S_1$ and $T_1$ excited states in order to allow an easy reverse intersystem crossing (RISC);
- Small overlap between HOMO-LUMO maintaining spatial separation of these orbitals in order to obtain valuable radiative decays;
- Introduction of intramolecular charge transfer (ICT) transitions by using donor-acceptor (D-A) structure alternating electron-rich and electron-deficient moieties, which has been proved to be an effective method to tune the band gap and to give rigidity to molecules;
- Structural rigidity and symmetry is required to attain a good emitter and an efficient ligand for the final assembly with Palladium cation.

Carbazole-based molecules meet most of these requirements and, consequently, have been widely used as TADF materials for various devices owing to their excellent hole transporting ability, good thermal stability and ease of formation of stable radical cations.

Also, the high triplet energy levels that arise the introduction of the planar and electron donating carbazole moiety is an issue of crucial importance to allow and enhance delayed fluorescence.[26]

These favorable properties introduce to the aim of this experimental work, which has been addressed to the design and the preparation of highly conjugated D-A carbazole-based molecules obtained from the functionalization at the N atom as well as the positions 3 and 6 of the carbazole core unit (Scheme 2).

In a successive stage, the target compounds will be submitted to complexation with Pd(II) ions in order to investigate their efficiency in the formation of self-assembled metalla-cages.

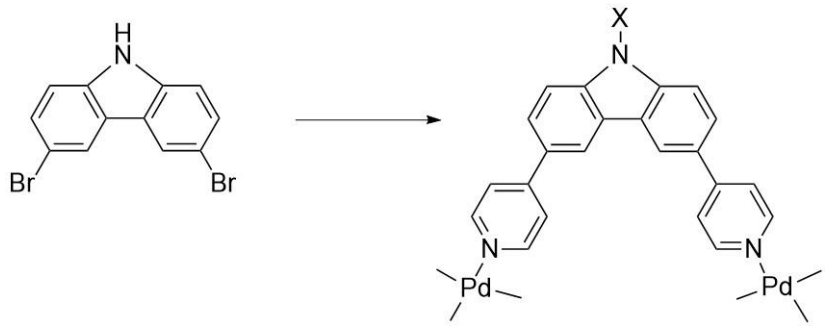


*Scheme 2. Final design of highly conjugated D-A carbazole-based molecules*

## *2.2 Synthesis of 3,6-dibromo-9H-carbazole*

Despite of the great potential of these symmetrical carbazole-ligands, their synthesis mostly requires corrosive, hazardous materials and harsh conditions or suffer from selectivity issues, thereby lowering the yield of the desired products. [27, 28]

However, the preparation of the target carbazole-based ligands has been attempted following two different synthetic routes, both of which involved the preparation of 3,6-dibromo-9H-carbazole as the potential building block prone to further functionalization both at the N-atom and at the positions 3 and 6 of the carbazole moiety.

In detail, the dibromo substituted carbazole was prepared upon reaction of a brominating agent such as N-Bromosuccinimide with carbazole. (Scheme 3).

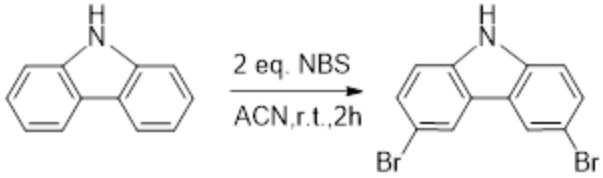


*Scheme 3 Synthesis of 3,6-dibromo-9H-carbazole*

Although the desired compound was isolated in high yield (87%), the whole process required careful optimization. Indeed, both the starting material and the brominated product were almost insoluble in different solvents at room temperature. In addition, further critical issue in the synthesis of such derivatives was represented by the obtainment of mono-brominated carbazole as the main side product. The low solubility of dibrominated product and the similar polarity between the impure mono-brominated compound and 3,6-dibromo-9H-carbazole made the purification via column chromatography quite tedious. Moreover, the yield of 3,6-dibromo-9H-carbazole strictly depends on the reaction time. In fact, if the reaction was carried out for more than two hours, other positions were activated towards radical bromination, as witnessed the loss of the symmetry in the $^{1}$H-NMR spectra of the final mixture.[29]

## *2.3 First Synthetic Route: Suzuki reaction*

At first, the strategy used was to replace both the bromides of 3,6-dibromo-9H-carbazole trough Suzuki coupling reaction with 4-Pyridinylboronic acid and $Pd(PPh_3)_4$ (i). Then, once the target compound was obtained, it could have been submitted towards functionalization on the –NH (ii) and thereafter $Pd^{2+}$ self-assembly reaction (iii).

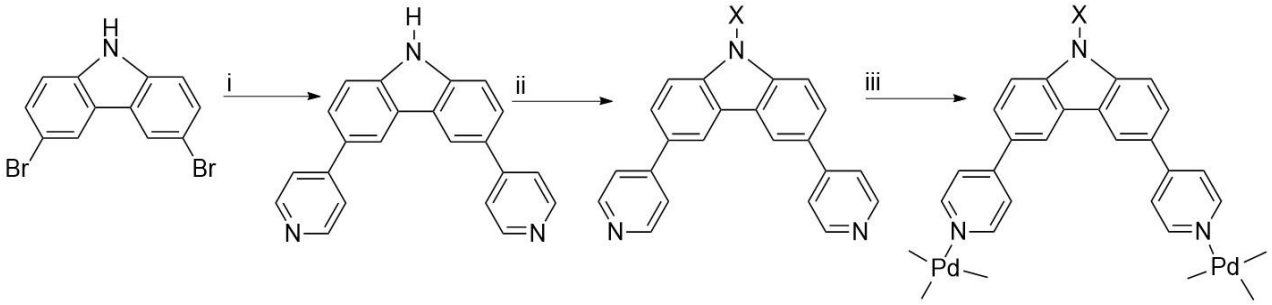


*Scheme 4. First Synthetic Route: Suzuki reaction*

Unfortunately, the initial step of this procedure –the double Suzuki coupling - was not successful since, even after running the reaction for long time at high temperatures, it was not possible to isolate the product arising from the cross coupling procedure. The purification of the crude mixture through chromatography column was inefficient because of the low amount of products and very low conversion. It was supposed that the presence of monobrominated carbazole in traces lowered the conversion and selectivity of the reaction. Moreover, the unprotected –NH in the presence of the potassium carbonate probably weakens the action of the $Pd(PPh_3)_4$ in the catalytic process with the boronic acid.

## *2.4 Second Synthetic Route: Functionalization of the –NH of 3,6-dibromo-9H-carbazole*

In a different approach, (route 2) the preliminary functionalization of the –NH was considered as the best option in order to synthetize the desired substrate. In this synthetic sequence, (i) 3,6-dibromo-9H-carbazole undergoes –NH functionalization then, (ii) the Suzuki coupling is performed and, finally (iii), the desired compound is allow to react with $Pd^{2+}$ .

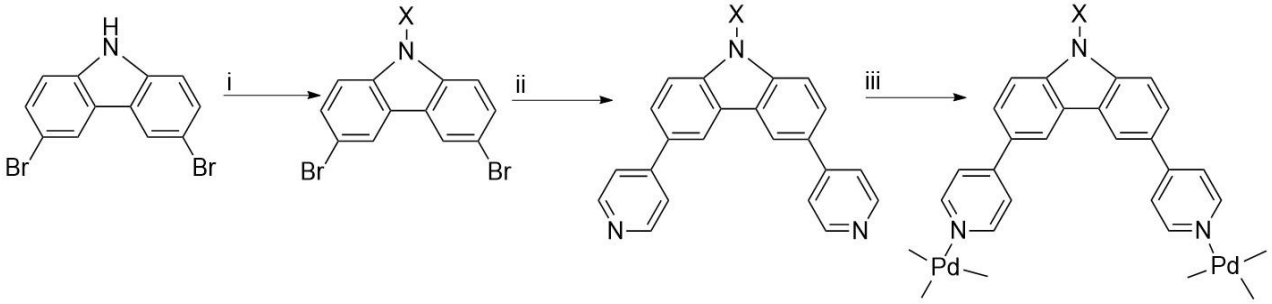


*Scheme 5 Second Synthetic Route: Functionalization of the –NH of 3,6-dibromo-9H-carbazole*

By following this pathway it was possible to get rid of traces of impurities, such as the unreacted mono-brominated carbazole, and no protection of the free –NH is required before heading to the Suzuki reaction.

The aim of the overall procedure is to obtain a compound with both electron-withdrawing and electro-donating moieties within the same molecule in order to allow reverse intersystem crossing and ICT transitions, as previously explained.[S1] Classical approaches to prepare N-arylcarbazoles includes the aromatic nucleophilic substitution reaction and copper-catalyzed Ullmann coupling reaction. However, reactions on carbazoles suffer of harsh conditions and low yields, in fact the production of the functionalized compounds was not straight given.

Carbazoles bearing electron-withdrawing substituents such as 3-bromo, 3,6-dibromo and 2,7-dibromo groups, show relatively low reactivity. Aryl halogens containing electron-withdrawing groups in para positions react with both electron-poor and electron-rich carbazoles to provide the N-arylcarbazoles in good yields. Aryl halogens bearing electro-donating groups show high reactivity with carbazoles containing electron-donating groups but exhibit lower reactivity with those containing electron-withdrawing groups.[30]

In this work; the 3,6-dibromo-9H-carbazole bears electron-withdrawing bromides and functionalization at the N-atom migh be undertaken by performing i) aromatic nucleophilic substitution reaction ($S_NAr$) with fluorobenzene substrate substituted in para with electron-withdrawing groups such as $NO_2$ and benzophenone and, ii) copper-catalyzed Ullmann coupling reaction with 4-Iodobenzene. Both of these protocols were evaluated in this experimental work.

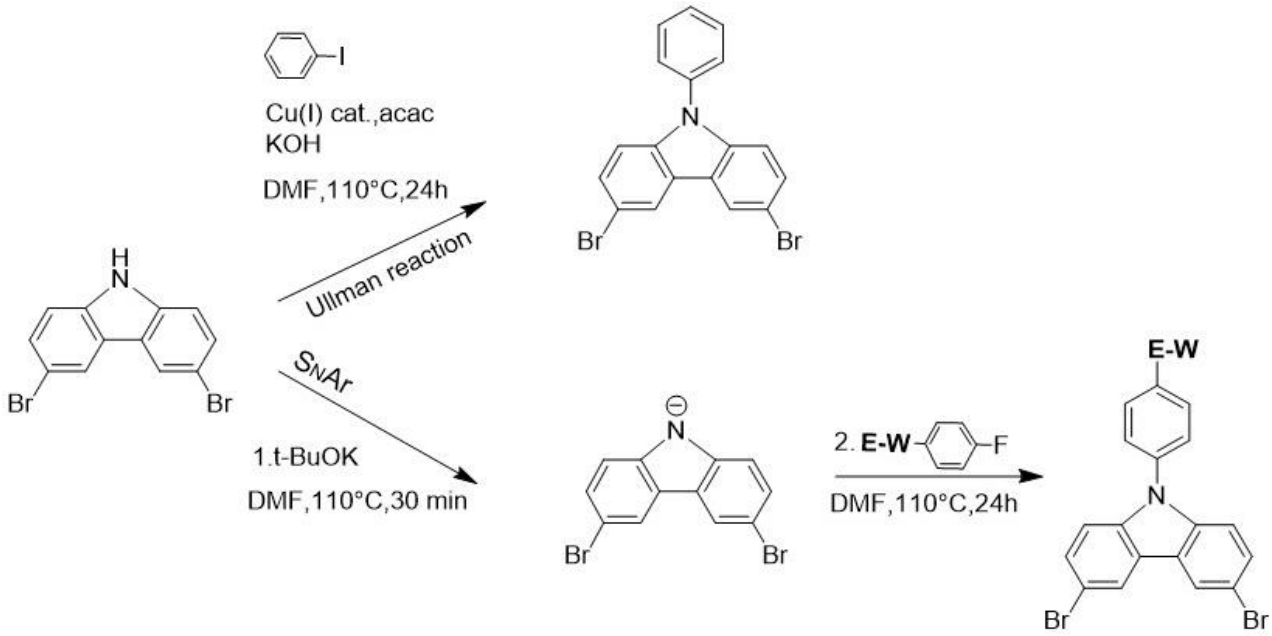


*Scheme 6 Functionalization of the –NH of 3,6-dibromo-9H-carbazole: i) $S_NAr$ and ii) Ullman reaction*

*2.4.1 Ullman reaction towards –NH of 3,6-dibromo-9H-carbazole*

Copper-catalyzed reaction has attracted considerable interest because copper is very inexpensive and undergoes desirable reactions for industrial applications. 3,6-dibromo-9-phenyl-9H-carbazole was obtained through cross-coupling reaction driven by Cu(I) and 2,2,6,6-tetramethylheptane-3,5-dione between the 3,6-dibromo-9H-carbazole and iodobenzene. The N-arylation of carbazole proceeds *via* a Cu(I) complex, which is generated *in situ* through the reaction of CuI with β-diketone. Consequently, the oxidative addition of iodobenzene onto the so obtained Cu(I) complex leads to a Cu(III) species. Then transmetallation between copper (III) complex and carbazole takes place to afford a copper (III) complex. Finally, copper (III) complex proceeds reductive elimination to provide the desired product while simultaneously releasing active copper (I) complex. The cross-coupling of iodobenzene with carbazole srongly depends on the nature of the solvent and, in our case, we have chosen to use dry N,N-dimethylformamide (DMF). Alsor, the choice of the appropriate base is an important factor that determines the efficiency of the copper-catalysed C-N bond formation reaction. [30]

At first, the procedure reported in literature was carefully reproduced without leading to appreciable results. Thus, the reaction conditions were slightly modified both by raising the temperature to 130°C from 90°C and by replacing the $Cu_2O$ with CuI as the Cu(I) source.

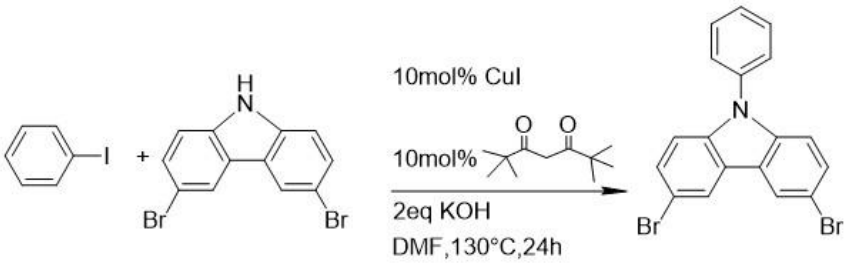


*Scheme 7 Synthesis of 3,6-dibromo-9-phenyl-9H-carbazole*

In this case, the desired product was isolated by flash column chromatography in moderate yield (40%).

The $^1$H-NMR(500 MHz, Chloroform-d) spectrum displays the signals characteristic of the carbazole moiety at ppm 8.22 (d, 2H), 7.68 – 7.61 (m, 2H), 7.28 (d, 2H), while the resonances of the protons related to the phenyl group are grouped in one multiplet at 7.56 – 7.50 (m, 5H).

*2.4.2 Aromatic nucleophile substitutions*

It was useful to synthetize 9-(4-nitrophenyl)-3,6-dibromo-carbazole (DNB) already reported in literature in order to find the best conditions for the previous Ullman copper reaction and to have guide lines for the purification of the next reaction with 4-fluorobenzophenone. Moreover, it was used to understand how reactivity towards the 3,6-dibromo-9H-carbazole depends not only on the aryl halogen used but also on the reaction conditions, such as temperature, solvents and base used.

The functionalization at the N-atom of 3,6-dibromo-9H-carbazole was also attempted through an of aromatic nucleophile substitution, SNAr.

The mechanism of aromatic nucleophile substitutions involves addition of the nucleophile followed by elimination of the leaving group; SNAr is a two-steps reaction in which the first one is rate determining. Accordingly, the addition of the nucleophile disrupts the aromaticity whereas during the elimination it is restored, thus the first one is the rate-determining step. Typical nucleophilic aromatic substitution have an halide as leaving group and a carbonyl or nitro group in ortho or para to the leaving group. An important requirement for the reaction to occur is that the anion formed by the nucleophilic attach is well stabilized trough electron withdrawing groups or resonance. In the investigated reaction, the C-F bond, that is a strong bond, characterizes both 4-Fluoronitrobenzene and 4-Fluorobenzofenone and it is difficult to break. In spite of this, fluoride accelerates the addition step because of its electronegativity, the polarization of the C-F bond through fluoride's inductive effect stabilizes the anionic intermediate, assists the acceptance of electrons by the benzene ring. Actually, the nitro group is very used so far because it is best at stabilizing the anionic intermediate; other electron-withdrawing groups are used as well, despite their reactivity. Sulfones, nitriles and keto groups are less efficient than nitro group indeed a ketone reacts is 80 time slower toward activation of the aromatic ring. However, these electron-withdrawing groups perform well when combined with a fluoride rather than a bromide as a leaving group; in addition, an anion stabilizing group in ortho or para to the potential leaving group can be used to facilitate the aromatic substitution.

*2.4.3 Synthesis of 9-(4-nitrophenyl)-3,6-dibromo-carbazole*

The synthesis of DNB by SNAr involved the preliminary deprotonation of –NH carbazole by potassium tert-Butoxide. Then, the reaction of the obtained anion with 4-fluoronitrobenzene was performed.[13]

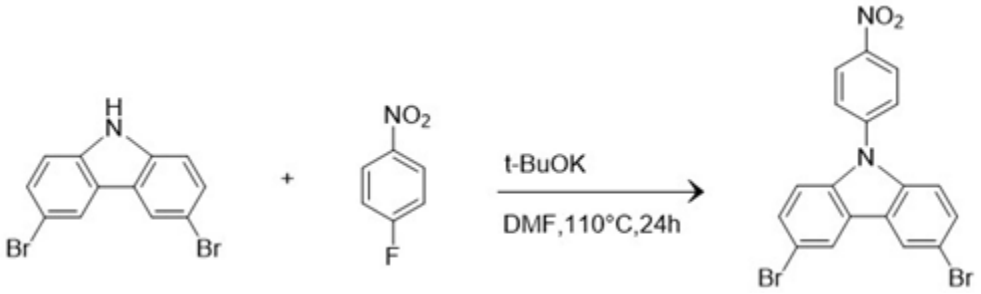


*Scheme 8 Synthesis of 9-(4-nitrophenyl)-3,6-dibromo-carbazole*

The crude residue was recrystallized from ethanol and the desired product was isolated (48% yield) without the need of chromatography work-up. The $^{1}$H NMR (500 MHz, Chloroform-d) spectrum presents peaks related to the protons of nitrobenzene at 7.77 (d, 2H) and 8.53 ppm (d, 2H).

Once the aromatic substitution worked successfully, DNB was submitted to Suzuki coupling. Unluckily, it was impossible to obtain a pure compound from the crude reaction mixture via chromatography column.

*2.3.4 Synthesis of (4-(3,6-dibromo-9H-carbazol-9-yl)phenyl)(phenyl)methanone*

Previous studies have shown that introduction of intramolecular interaction may afford modulation of molecular energy levels and favors effective electronic communication within molecules. To verify this idea it was adopted an D-A structure, in which 3,6 -dibromo-9H-carbazole was functionalized on the N position with benzophenone (BP), a very strong electron acceptor group, in order to obtain (4-(3,6-dibromo-9H-carbazol-9-yl)phenyl)(phenyl)methanone.[26] Combination of 3,6-dibromo-9H-carbazole and BP attributes remarkably rigidity to the final structure because of the intramolecular D-A contacts between the mentioned moieties.

The SNAr reaction between 4-Fluorobenzophenone and 3,6-dibromo-9H-carbazole is performed after deprotonation of the –NH by potassium tert-Butoxide. The temperature of the reaction was increased from 110 to 150°C since 4-Fluorobenzophenone is less reactive than 4-Fluoronitrobenzene. The product was recrystallized from EtOH and the expected product was collected as white powder ( 44% yield).

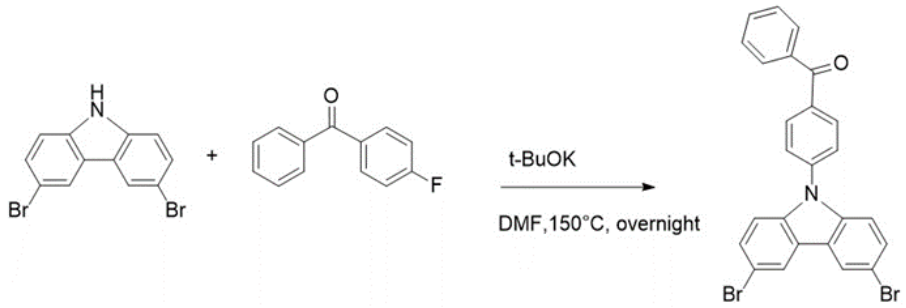


*Scheme 9 Synthesis of (4-(3,6-dibromo-9H-carbazol-9-yl)phenyl)(phenyl)methanone*

The $^{1}$H-NMR (500 MHz, Chloroform-d) presents at ppm 8.26 – 8.22 (d, 2H), 7.95 – 7.90 (dd, 2H) and 7.39 (d, 2H). the typical peaks corresponding to the 3,6-dibromocarbazole moiety It is worth noting that the signals of the phenyl ring attached to the nitrogen are grouped in one multiplet at ppm 7.60 – 7.55 (m, 4H). The multiplet at 7.71 – 7.65 (m, 3H) was assigned to the outlying protons of the further phenyl ring. In addition, the couple of protons of the same aromatic ring are shifted to lower field between ppm 8.12 – 8.08 (m, 2H) because of their lower electron-density. The keto-group was identified at ppm 195.45 in the $^{13}$C NMR (500 MHz, Chloroform-d) spectrum.

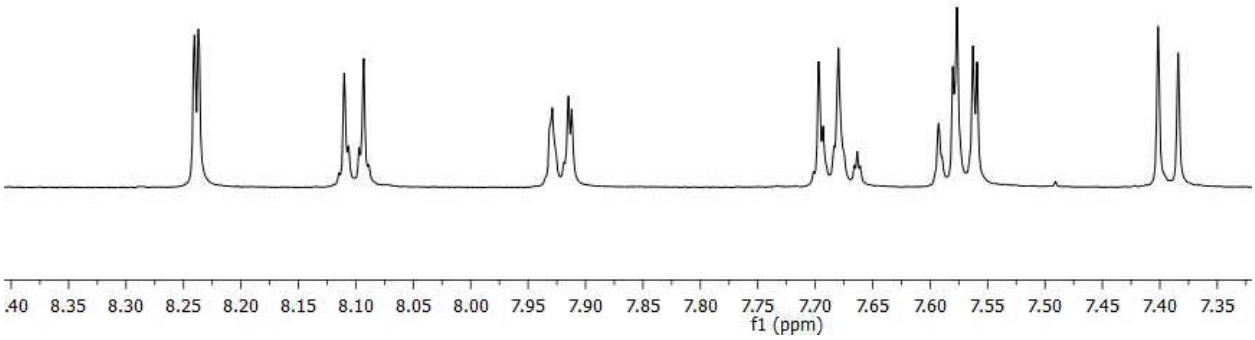


*Figure 9 $^{1}$H-NMR spectrum of (4-(3,6-dibromo-9H-carbazol-9-yl)phenyl)(phenyl)methanone in $CDCl_3$*

In contrast to all previous attempts, the Suzuki coupling was successfully performed on (4-(3,6-dibromo-9H-carbazol-9-yl)phenyl)(phenyl)methanone.

*2.4.4 Suzuki reaction on 4-(3,6-dibromo-9H-carbazol-9-yl)phenyl)(phenyl)methanone*

(4-(3,6-di(pyridin-4-yl)-9H-carbazol-9-yl)phenyl)(phenyl)methanone and (4-(3,6-di(pyridin-3-yl)-9H-carbazol-9-yl)phenyl)(phenyl)methanone were synthetized through Pd(0)-catalysed cross-coupling reaction. The Suzuki Cross-coupling reaction of Boronic acid with halides has different advantages and it is widely used in organic industrial and academic laboratories. The mechanisms of cross-coupling starts with Oxidative addition of the aromatic halide to the initial Palladium (0) phosphine complex to form a Palladium (II) intermediate. This then undergoes a transmetallation with the boronic acid, the nucleophilic aromatic ring of the boronic acid is transferred into the palladium complex and the counter halide anion moves in the opposite direction. The new complex with two organic ligands undergoes reductive elimination to give the coupled product and the Palladium (0) catalyst, ready for another cycle. The slow step of the cycle is the transmetallation; the reaction indeed needs an additional base to accelerate this step. The base reacts with the Boron forming a nucleophilic "ate" complex which facilitates transmetallation with Pd(II)-halide complex, because the Boron is electronically saturated. In this work, $CsCO_3$ had been chosen as base because it was reported in literature and different experiments did not work, unless there was no strong base in the reaction mixture. The synthesis of symmetrical carbazole-based Ligand precursors implies limitations, the mono-substituted compound are obtained as side products in all cases.[28]

At first (4-(3,6-di(pyridin-4-yl)-9H-carbazol-9-yl)phenyl)(phenyl)methanone was synthetized using an excess of 4-Pyridinylboronic acid in the presence of a strong base as $Cs_2CO_3$ and $Pd(PPh_3)_4$ as a catalyst. The reaction needs temperature as high as105°C and prolonged time of reaction (72h) before work up. The reaction was monitored by $^1$H-NMR analysis; it was observed how the intensity of the peaks related to the boronic acid decreased with the conversion of the starting material. The purification of the crude was tricky and it was used a flash chromatography column with an eluent mixture of 3:1 $CH_2Cl_2$/Hexane with $Et_3N$ 40% vol., the issue of separation is to get rid of the (4-(3,6-dibromo-9H-carbazol-9-yl)phenyl)(phenyl)methanone that undergoes the a single cross-coupling.. The product was isolated as a yellow powder (55.4 % yield).

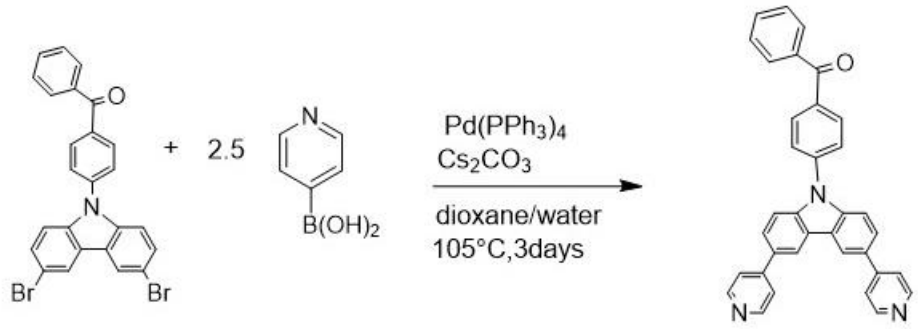


*Scheme 10 Synthesis of (4-(3,6-di(pyridin-4-yl)-9H-carbazol-9-yl)phenyl)(phenyl)methanone*

In the $^{1}H$ NMR (500 MHz, Chloroform-d) spectrum revealed the signals of the (4-(3,6-dibromo-9H-carbazol-9-yl)phenyl)(phenyl)methanone shifted to lower ppm and the Hα and Hβ protons of the the pyridines were respectively assigned at ppm 8.74 – 8.70 (dd, 4H) and 7.82 – 7.77 (m, 4H).

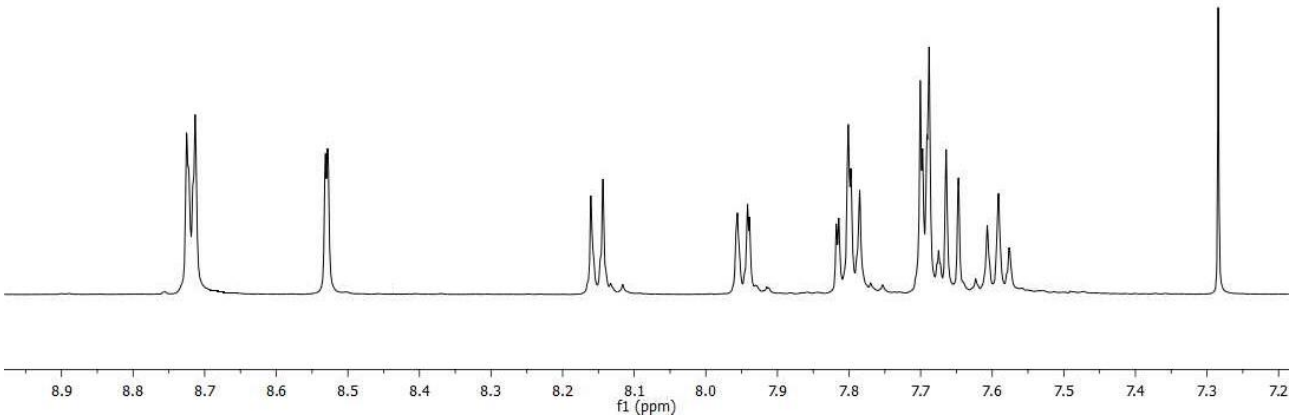


Figure 10 *$^{1}H$-NMR spectrum of (4-(3,6-di(pyridin-4-yl)-9H-carbazol-9-yl)phenyl)(phenyl)methanone in $CDCl_3$*

*2.4.5 Suzuki reaction on 4-(3,6-dibromo-9H-carbazol-9-yl)phenyl)(phenyl)methanone*

Then the Suzuki coupling reaction was performed with an excess of 3-Pyridinylboronic acid on (4-(3,6-dibromo-9H-carbazol-9-yl)phenyl)(phenyl)methanone, following the same reaction procedure. A yellow powder was isolated (55.4% yield).

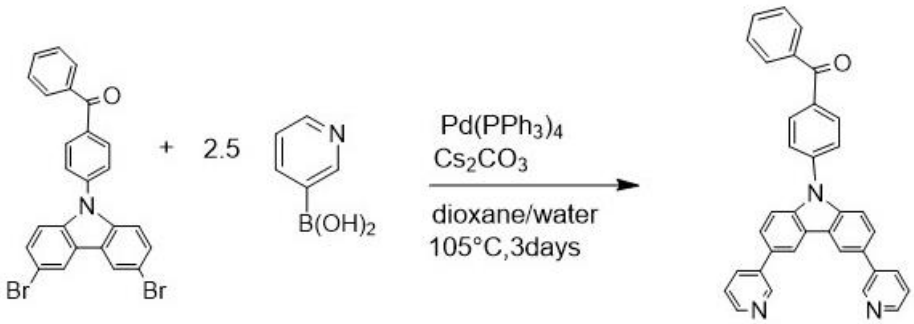


*Scheme 11 Synthesis of (3-(3,6-di(pyridin-4-yl)-9H-carbazol-9-yl)phenyl)(phenyl)methanone*

3-Pyridinylboronic and 4-Pyridinylboronic showed the same reactivity and conversion, the separation procedure was as tricky as the previous reaction and it was used the same eluent mixture for the chromatography column. The $^{1}$H NMR (500 MHz, Chloroform-d) spectrum presented the Hα at ppm 9.03 – 9.01 (dd, 2H), the Hα close to Hβ at 8.66-8.64 (dd, 2H), the Hβ at 7.46 – 7.43 (dd, 2H) and the last Hδ at 7.75-7.72(dd, 2H). the protons related to the phenyl group attached to the nitrogen are split into two groups of signals integrating two at ppm 8.07-8.04 and 7.62-7.57 (m,2H), 7.83-7.79 (m, 2H),

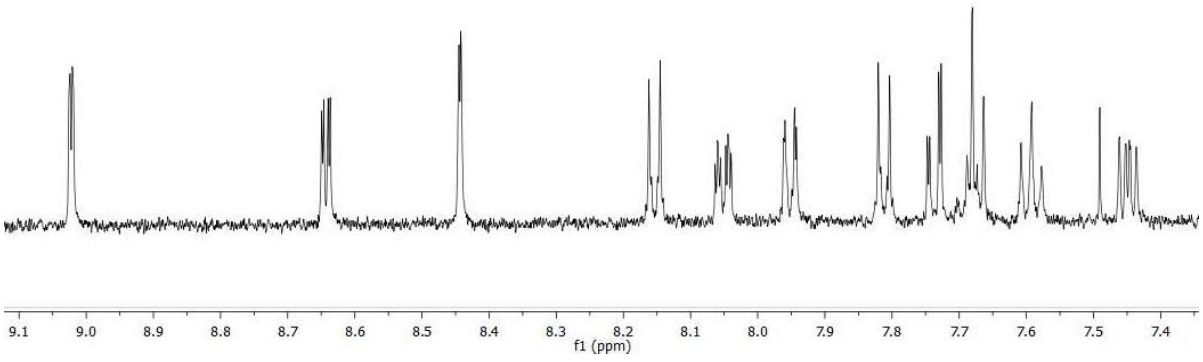


*Figure 11 $^{1}$H-NMR spectra of (3-(3,6-di(pyridin-4-yl)-9H-carbazol-9-yl)phenyl)(phenyl)methanone in $CDCl_3$*

## *2.5 Synthesis of supramolecular cage with $Pd^{2+}$ and (4- and (3-(3,6-di(pyridin-4-yl)-9H-carbazol-9-yl)phenyl)(phenyl)methanone*

The synthesis of supramolecular structures is driven by geometric design principles, and as with synthetic organic chemistry, the rules governing the reactivity of many systems are understood such that a desired product can often be obtained. However, unlike classical organic synthesis, where reactions are performed one after the other under kinetic control, supramolecular synthesis relies on reactions which proceed under thermodynamic control, such that 'annealing' or 'error checking' processes may proceed to break down less stable products in favour of more stable ones. Geometric design principles focus on coordinative interactions between organic ligands and metal ions, and do not consider interactions between ligands within an architecture, thus new supramolecular assemblies are mostly obtained by serendipity rather than accurate scientific planning.

Accordingly, (3- and (4-(3,6-dibromo-9H-carbazol-9-yl)phenyl)(phenyl)methanone were allowed to react with an excess of $[Pd(CH_3CN)_4BF_4]^{2-}$ in DMSO-d6 for 2 days at 80°C under nitrogen atmosphere(scheme 12).[31]

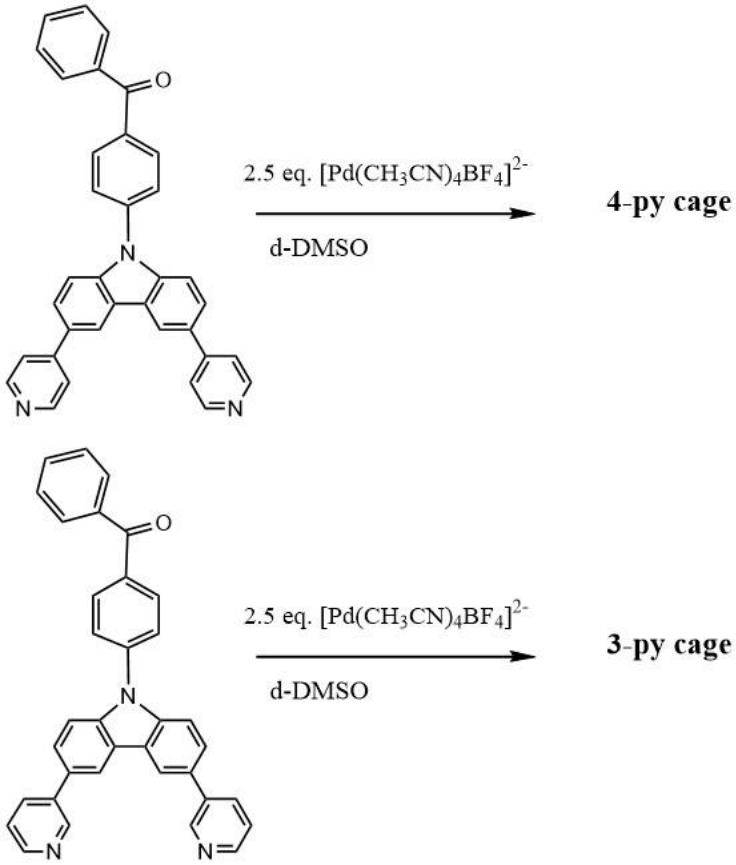


*Scheme 12 Synthesis of Pd(II) complexes with (4- and (3-(3,6-di(pyridin-4-yl)-9H-carbazol-9-yl)phenyl)(phenyl)methanone*

In both cases, a dark-brown mass was collected after cooling at 0°C the reaction mixtures.

Our strategy is characterized by the use of a metal-directed assembly in which naked divergent metals are combined with more complicated nitrogen-containing ligands. It is well-known that Pd(II)–pyridine coordination bond is reversible, in fact during these self-assembly processes, many reversible reactions may occur in parallel until the system reaches equilibrium, and thermodynamically stable products might be formed in near- quantitative yield.

The formation of roughly spherical polyhedral with formula $M_nL_{2n}$ is predicted when metal ions with square planar coordination sphere (M) and rigid bent ligands (L) are mapped onto the vertices and edges of the polyhedral. For entropically favored regular or semiregular polyhedral, n is limited by geometrical constrains to be 6, 12, 24 or 30 (and on).[7]

Many authors cite that a small initial difference in the angle formed between the two coordinating pyridine rings of the bidentate ligands leads to an incommensurate differences in the resultant structures.[32,33, 25,23, 24]

The crystal structures of both (4- and (3-(3,6-dibromo-9H-carbazol-9-yl)phenyl)(phenyl)methanone were obtained by X-Ray analysis. Since the bridging angles between the Nitrogen of the pyridines are 92.50° and 106.86°, their reactivity towards $Pd^{2+}$ is expected to be different.

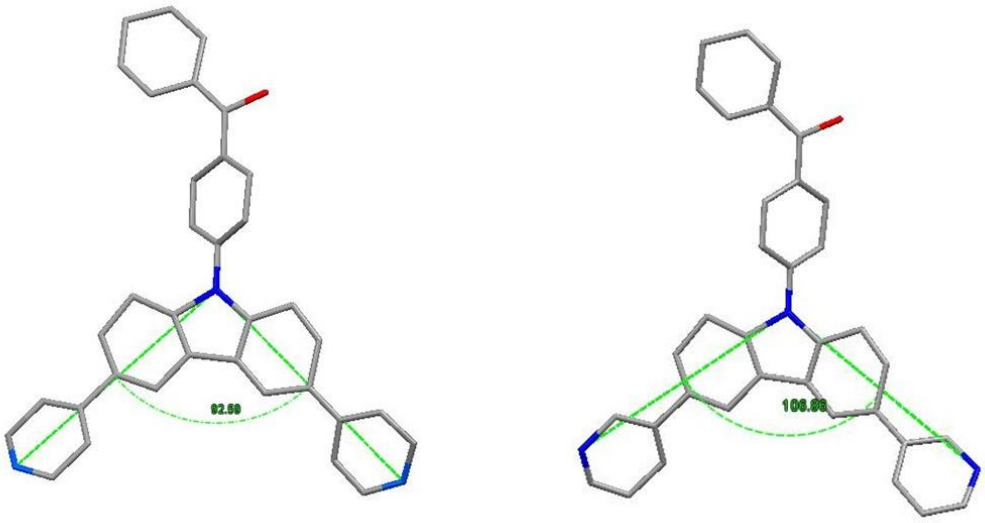


*Figure 12. X-ray single crystal structure of (4- and (3-(3,6-dibromo-9H-carbazol-9-yl)phenyl)(phenyl)methanone*

According to literature, the polyhedral expected from (4- (3,6-dibromo-9H-carbazol-9-yl)phenyl)(phenyl)methanone should be characterized by more complicated structure that the one obtained from (3-(3,6-dibromo-9H-carbazol-9-yl)phenyl)(phenyl)methanone.

Usually for wider bridging angles the complexation with $Pd^{2+}$ leads to a simple "paddle wheel" structure, where the net charge of the complex spans between 2+ and 4+ and the number of monomeric units within the cage framework is restrained.[34]

On the contrary, if the bridging angle is smaller the resulting complex structures bear much higher global charge (12+), witnessing the assembly of a higher number of monomeric units. [24, 25]

The reaction between (4- and (3-(3,6-di(pyridin-4-yl)-9H-carbazol-9-yl)phenyl)(phenyl)methanone and $[Pd(CH_3CN)_4BF_4]^{2-}$ was checked by $^1$H-NMR analysis. The strategy was to compare the differences between the signals of (4- or (3-(3,6-di(pyridin-4-yl)-9H-carbazol-9-yl)phenyl)(phenyl)methanone in DMSO-d6 and the ones of the compound obtained in the reaction mixture. Referring to (4- and (3-(3,6-di(pyridin-4-yl)-9H-carbazol-9-yl)phenyl)(phenyl)methanone as AP013 and AP021 respectively the corresponding cages were renamed AP019 and AP022, in order to simplify the discussion of the synthesis and characterization.

*2.5.1 Supramolecular complexation of Pd(II) towards 4-pyridyne ligand.*

It is here reported in Figure 13 the $^{1}$H-NMR spectra of the (4-(3,6-di(pyridin-4-yl)-9H-carbazol-9-yl)phenyl)(phenyl)methanone (AP013) and after reaction with $[Pd(CH_3CN)_4BF_4]^{2-}$ (AP019).

In the $^{1}$H-NMR spectrum of AP019, especially at ppm 8.68-8.72 and 9.02-9 the peaks present very broad profiles, these signals are respectively related to the Hα pyridine protons and the isolated proton of the carbazole. In addition, the signals related to the Hβ pyridine protons are broader compared to the free ligand spectrum.

According to literature, [7] it is indicative of a quite large complex because it has already been reported that those protons present broad signals when complexed with Pd(II).

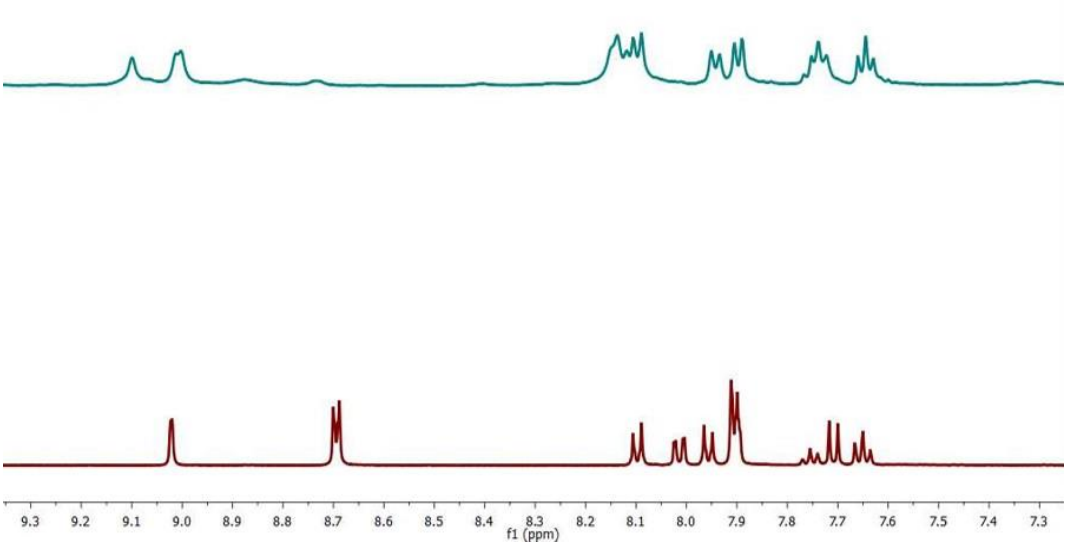


*Figure 13 $^{1}$H-NMR spectra of AP013 (red) and AP019 (green) in DMSO-d6*

When the 4-pyridine ligand is complexed with palladium cations the tumbling motion of its protons is slower on NMR time scale.

Diffusion-ordered NMR spectroscopy (DOSY) evinced a single product with a band at diffusion coefficient of $9.1 \times 10^{-11}$ $m^2/s$.

DOSY $^{1}$H-NMR spectroscopy was used to compare the diffusion coefficient of (4-(3,6-di(pyridin-4-yl)-9H-carbazol-9-yl)phenyl)(phenyl)methanone (AP013) and AP019, respectively $1.7 \times 10^{-10}$ $m^2/s$ and $9.1 \times 10^{-11}$ $m^2/s$ as shown in Figure 14.

The remarkable difference between the two values of diffusion coefficients is indicative of a much larger structure, which results from the complexation of the ligand towards $Pd^{2+}$.

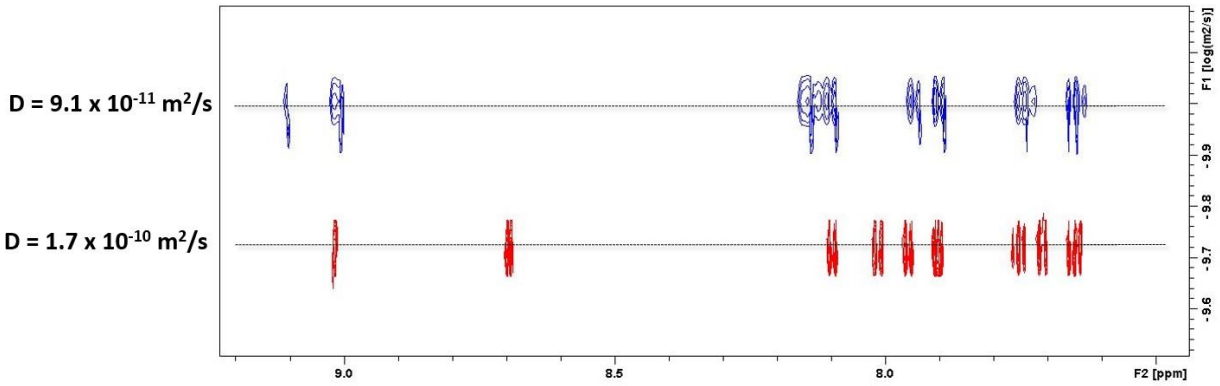


*Figure 14 DOSY $^{1}$H-NMR spectra of AP013 (red) and AP021 (bue) in d-DMSO with the corresponding Diffusion coefficients.*

A High Resolution Electrospray Ionization (HR-ESI) was recorded at the University of Leeds on a Bruker MaXis Impact instrument in positive ion mode thanks to the work of PhD Diego Rota Martir member of Eli Zysman-Colman group of the University of Saint Andrews.

The sample was injected by direct infusion from a DMSO solution of a concentration of 1 x $10^{-4}$ M.

The HR-ESI analysis results (Figure 15) suggest that the cage AP019 might correspond to a complex with a stoichiometry of $[Pd_6L_{12}](BF_4)_{12}$.

Three fragmentation peaks in the reported experimental mass spectrum (in black) with the charge state +8, +7 and +6 might correspond to the loss of 6 ,7 and 8 units of $BF_4^-$ ions. In this case , the expected palladium complexes are $[Pd_6L_{12}](BF_4)_4^{8+}$ , $[Pd_6L_{12}](BF_4)_5^{7+}$ and $[Pd_6L_{12}](BF_4)_6^{6+}$. However, the experimental peaks at 879.81 m/z (charge state +8), 1056.0 m/z (+7), 1184.0 m/z (+6) do not match perfectly the theoretical simulated spectra for each state of charge.

In spite of this, the isotopic distribution of the charge 8+ and 7+ matches the behavior expected by palladium isotopes.

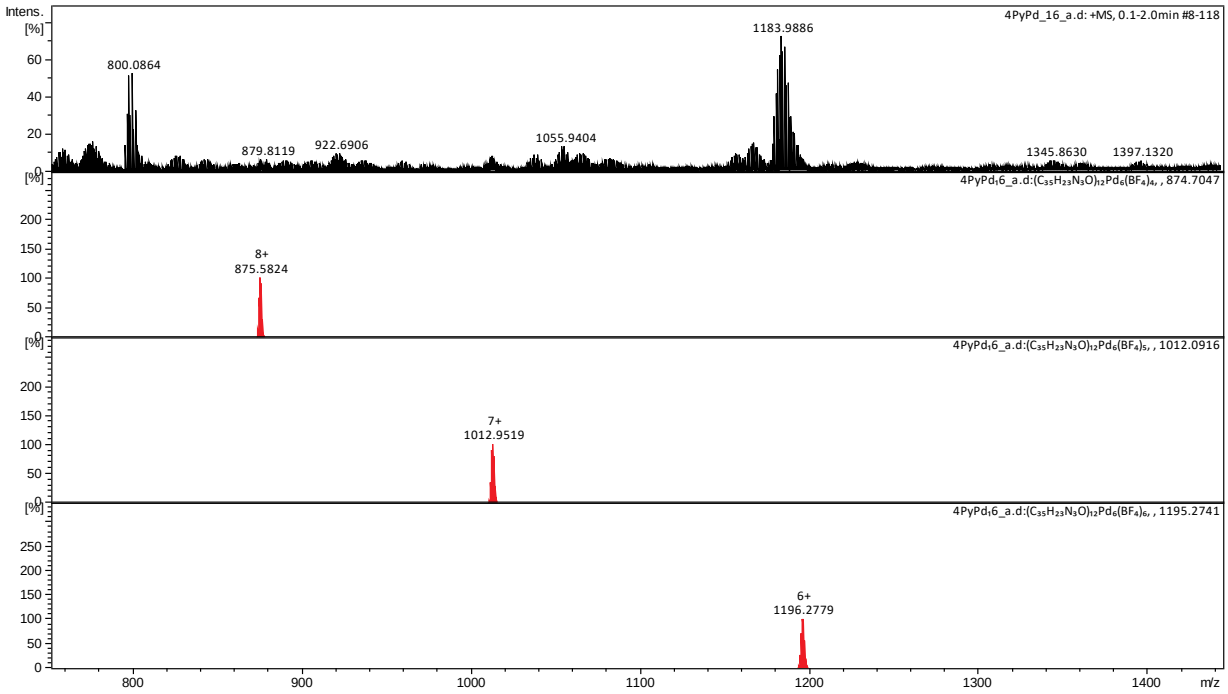


*Figure 15 A High Resolution Electrospray Ionization (HR-ESI) of AP019 in DMSO (1 x $10^{-4}$ M).*

Further studies are programmed to increase the quality of the mass spectrum and to decrease the differences between theoretical and obtained values, in spite of this the HR-ESI reported above is considered to be a reliable evidence of the formation of a large complex whose monomeric unit contains $[PdL_2](BF_4)_2$ .

*2.5.2 Supramolecular complexation of Pd(II) towards 3-pyridine ligand*

The reaction between (3-(3,6-di(pyridin-4-yl)-9H-carbazol-9-yl)phenyl)(phenyl)methanone and $[Pd(CH_3CN)_4BF_4]^{2-}$ was not successful as the previous one. It was already supposed that the larger bridging angle had to bring to a different structure than what expected with the other ligand.

It is here reported in Figure 16 the $^1$H-NMR spectra of the (3-(3,6-di(pyridin-4-yl)-9H-carbazol-9-yl)phenyl)(phenyl)methanone (AP021) and after reaction with $[Pd(CH_3CN)_4BF_4]^{2-}$ (AP022).

In the $^1$H-NMR spectrum of AP022, all the signals seem to be broader compared to the spectrum of the 3-pyridine free ligand.

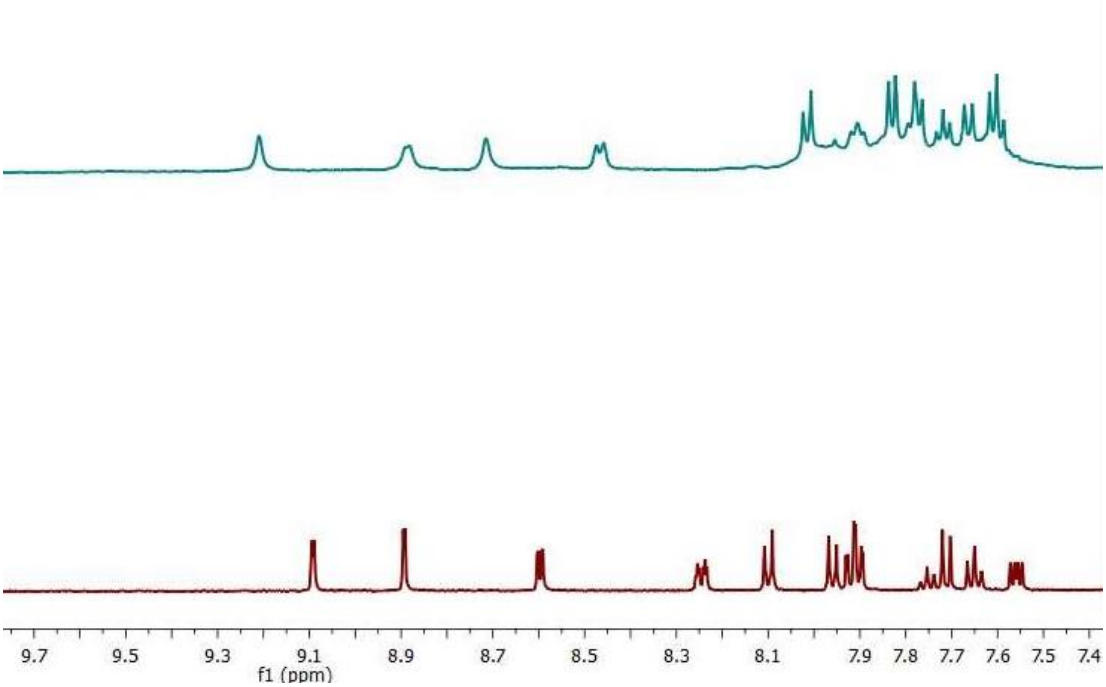


*Figure 16 $^1$H-NMR spectra of AP021 (red) and AP022 (green) in DMSO-d6*

In spite of this, no data dealing with DOSY spectroscopy resulted to be valuable to evince the formation of a supramolecular system toward Pd(II).

Further studies have been programmed to obtain a valid HR-ESI spectrum.

## *2.6 Photophysical Properties*

The relevant Photophysical data of the ligands AP013 and AP021 and the corresponding complexes AP019 and AP022 are summarized in Table 1

*Table 1 Photophysical Properties in DCM solutions*

| | **Absorption** | **Emission 298 K**[a,b] | | | | |
|---|---|---|---|---|---|---|
| **Compound** | λmax (nm);ε ($M^{-1}$ $cm^{-1}$) | λ(nm) | τ (ns)dear | τ (ns)air | $\phi_P$(%)dear | $\phi_{PL}$(%)air |
| AP013 | 258(13204) 299(10614) 324(7067) 341(5853) | 476 | 18(38), 9512 (62) | 3(100) | 52.0 | 10.0 |
| AP021 | 260(5479) 297(101773) 344(41918) 355(39276) | 498 | 11 (87), 15825(13) | 13(100) | 56.3 | 18.2 |
| AP019 | 277(129022) | 466 | 3 (100) | 5(87), 16(13) | 3.3 | 1.3 |
| AP022 | 278(277778) 343(208889) | 490 | 14 (78), 24201(21) | 13(100) | 2.6 | 1.6 |

[a] Measurements in degassed DCM at 298 K ($\lambda_{ex}$ = 360 nm). [b] $\Phi_{PL}$ measurements were carried out in degassed DCM under nitrogen or oxygen equilibrated atmosphere ($\lambda_{exc}$ = 360 nm) using quinine sulfate as the external reference ($\Phi_{PL}$ = 54.6% in 0.5 M $H_2SO_4$ at 298 K).

*2.6.1 AP013 and AP021 Absorption Spectroscopy*

The absorption spectra were recorded at room temperature from diluted ($10^{-5}$ M) solutions of DCM. The ligands AP013 and AP021 display similarly shaped absorption profiles, with the one relative to AP013 slightly red shifted with respect to that of AP021.

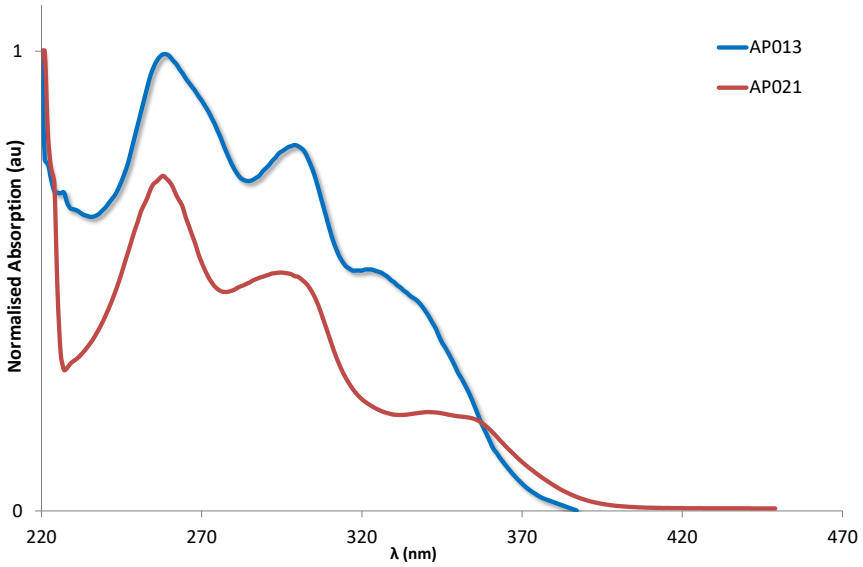


*Figure 17 Absorption spectra of AP013 and AP021 in DCM ($10^{-5}$ M)*

Upon passing from dichloromethane (DCM) to a more polar solvent such as acetonitrile, the absorption profile of AP013 undergoes to a pronounced bathochromic shift, while the one relative to AP021 does not show appreciable variations. This feature might suggest a more evident charge-transfer (CT) character of the transitions observed for AP013 rather than those of AP021.

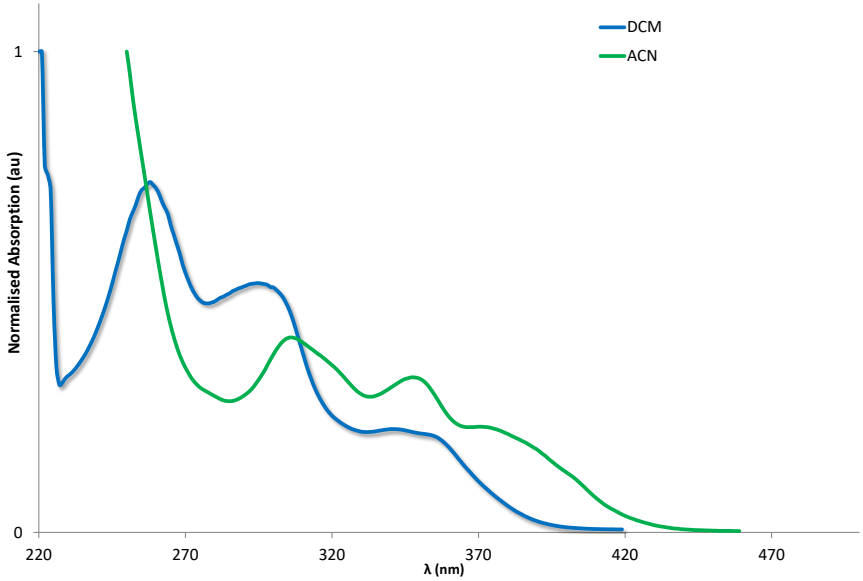


*Figure 18 Absorption spectra of AP013 in DCM(blue) and in ACN (green) ($10^{-5}$ M)*

The positive solvatochromism (Figure 18) that is experienced by AP013 is also evident when cuvettes containing diluted DCM or ACN solutions of AP013 are exposed to UV lamp (λexc = 365nm). The DCM solutions displays blue emission, while green colour is observed from the one relative to the same sample dissolved in ACN.

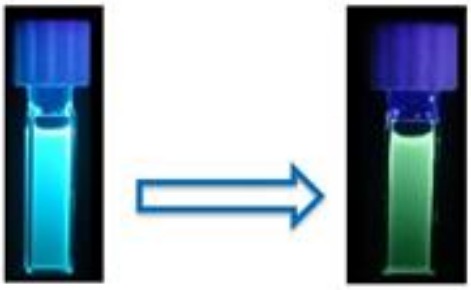

*Figure 19 AP013 in DCM solution (left) and AP013 in ACN solution (right) exposed to UV lamp light*

### *2.6.2 AP019 and AP022 Absorption Spectroscopy*

The absorption profiles of the ligands AP013 and AP021 underwent significant modification upon complexation with Pd(II) to form the complexes AP019 and AP022, respectively. In the case of AP019, an intense transition centred at ca. 275 nm was detected, and the structured profile displayed by the parent ligand AP013 was no longer observed. Relative to comparison of the spectrum of AP022 with the one of the parent ligand AP021, it can be observed how the complexation with Pd(II) led to the blue shift of the transitions occurring at λ>290 nm.

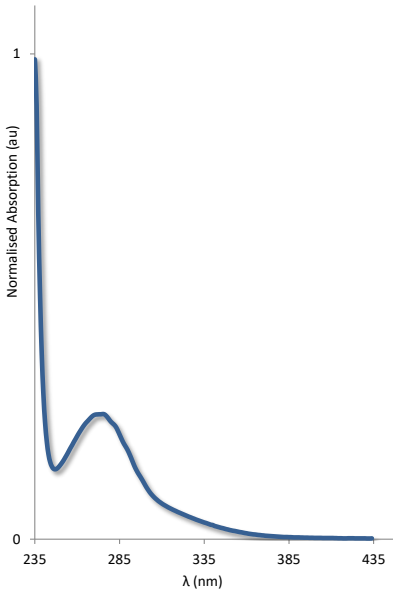


*Figure 20 Absorption spectrum of AP019 in DCM ($10^{-5}$ M)*

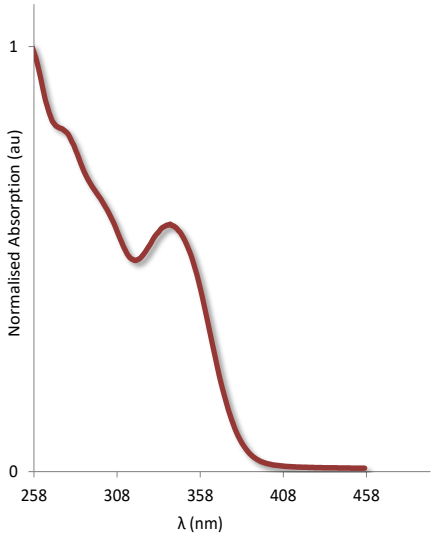


*Figure 21 Absorption spectrum of AP022 in DCM ($10^{-5}$ M)*

*2.6.3 AP013 and AP021 Steady State Emission properties*

The steady state emission spectra and time-resolved experiments were performed at 298 K. Relative to steady state emission spectra, upon excitation ($\lambda_{exc}$ = 360 nm) of the diluted DCM solutions, the free ligands AP013 and AP021 displayed broad and unstructured profiles centred at 480 and 498 nm, respectively.

The photoluminescence quantum yield (PLQY) values of AP013 and AP021 (Table 1) were found to increase significantly after removal of dissolved $O_2$. In particular, the PLQY of AP013 varied from 10 to 52 % and, similarly, AP021 displayed an increment from 18 to 56%. This evidence suggests the presence of excited states with triplet multiplicity for both ligands.

In addition, the resolved measurements performed on the degassed solutions of the free ligands provided decays that, in most cases, were best fitted with bi- or multiexponential functions in which the component in the microseconds range (Table 1) was more relevant for AP013 (62.5%) with respect to that of AP021 (13%). It is worth noting that the lifetime decays obtained from air-equilibrated solutions of AP013 and AP021 were best fitted, in both cases, with monoexponential functions with lifetimes in the tenth of nanonoseconds range.

Relative to steady state emission spectra, upon excitation ($\lambda_{exc}$ = 360 nm) of the diluted ACN solutions, the free ligands AP013 and AP021 displayed broad and unstructured profiles centred at 506 and 534 nm, respectively. If compared to the data obtained from DCM solutions, the profiles of AP013 and AP021 are both centred at lower energies,suggesting therefore the stabilization of polar CT states on passing from DCM to ACN.

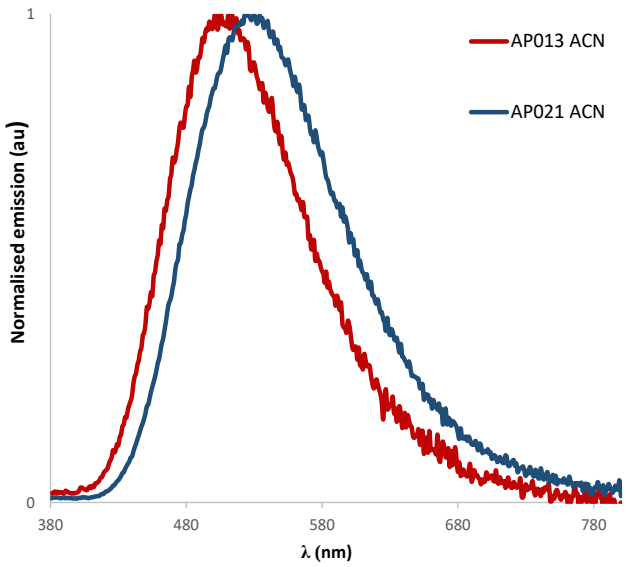

The photoluminescence quantum yield (PLQY) values were found to increase after removal of dissolved $O_2$ from the DCM solutions of AP013 and AP021. In particular, the PLQY of AP013 varied from 17% to 30% and AP021 from 13%. to 35% (Table 2).
However, by the comparison of the PLQY values of AP013 and AP021 in DCM and ACN degassed solutions, it can be observed that the PLQY values of both free ligands decrease moving on more polar solvent of 20% on the total percentage yield.

*Table 2 Photophysical Properties in ACN solutions*

| | **Absorption** | **Emission 298 K**[a,b] | | |
|---|---|---|---|---|
| **Compound** | λmax (nm);ε ($M^{-1}$ $cm^{-1}$) | λ(nm) | $\phi_P$(%)dear | $\phi_{PL}$(%)air |
| AP013 | 310 (11245)<br>351(9030)<br>379(5965)<br>419(1450) | 506 | 27.4 | 17 |
| AP021 | 258 (27325)<br>298(25275)<br>340(8168)<br>358 (6831) | 534 | 34.7 | 13.4 |

[a]Measurements in degassed MeCN at 298 K ($\lambda_{exc}$ = 360 nm).[b] $\phi_{PL}$ measurements were carried out in degassed MeCN under nitrogen or oxygen ($\lambda_{exc}$ = 360 nm) using quinine sulfate as the external reference ( $\phi_{PL}$ = 54.6% in 0.5 M $H_2SO_4$ at 298 K).

*2.6.4 AP019 and AP022 steady state emission spectra*

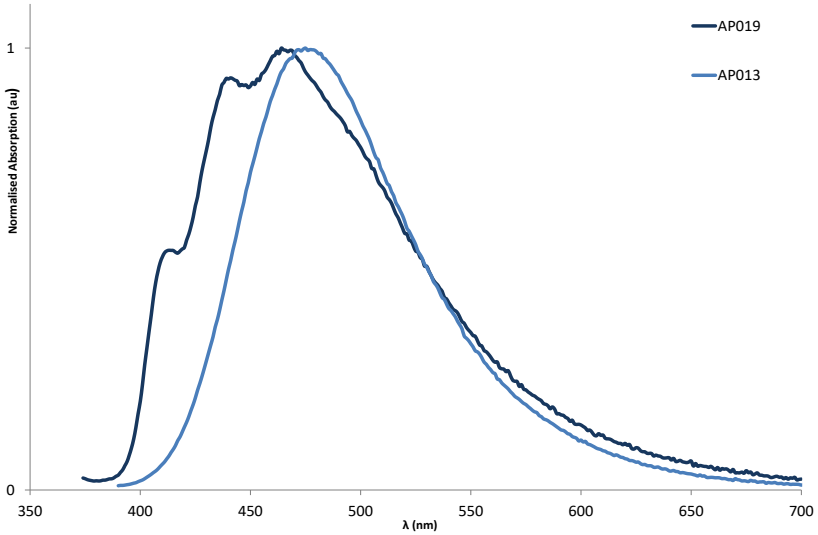


*Figure 22 Emission spectra of AP013 and AP019 in DCM ($10^{-5}$ M)*

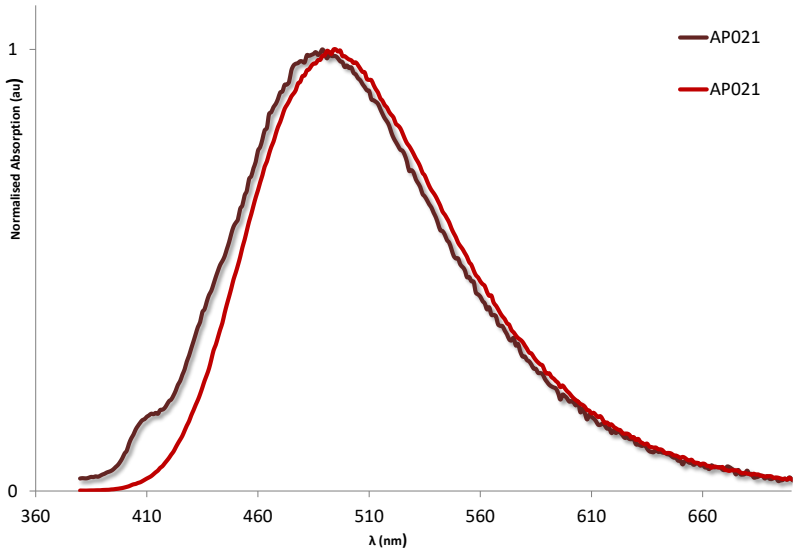


*Figure 23 Emission spectra of AP021 and AP022 in DCM ($10^{-5}$ M)*

Upon excitation of the corresponding diluted DCM solutions, both complexes, namely AP019 and AP022, display emission maxima that are slightly blue shifted with respect to the parent free ligands AP013 and AP021, respectively.

This effect might be due to the ensuing positive net charge of the complexes and to the lowering of the π-conjugation along the ligands occurring upon complexation.

PLQY and lifetime decays were checked in solution state in order to evaluate the efficiency in emission of the species and to characterize their properties (table 1).

In contrast to the free ligands, the removal of dissolved $O_2$ from DCM solutions of AP019 and AP022 did not result in any appreciable increase of the PLQY values, which remains almost unaltered and quite low for both the complexes.

Relative to lifetime measurements, the microsecond component that was displayed by AP013 was no longer observed from AP019; in both degassed and aerated solutions of AP019, the emission lifetime shows the presence of a sole fast fluorescent decay in the scale of nanoseconds.

On the other hand, no particular differences were detected from the analysis of the lifetime decay of AP022 with respect to AP021. In fact, both AP021 and AP022 in degassed solutions similarly present an emission characterised for the 80-90% by a short decay and for the remaining 30-20% by a longer decay in the scale of microseconds. In AP022 aerated solutions the longer decay completely disappears in favour of a fast decay.

It can be deduced that complexation of AP013 with Pd(II) ions reduces almost completely the population of the excited states with triplet multiplicity that were detected in the free ligand.

In contrast, the same complexation reaction performed onto AP021 seems not to turn in the quenching of triplets states to the same extent as that observed for AP013.

## *2.7 Solid state emission properties*

Solid state emission spectroscopy was performed at room temperature on both AP013, AP021 and the corresponding complexes using PMMA doped thin films formed by spin coating.

*Table 3 Photophysical properties in solid state*

| Compound | Emission 298 K[a] | | |
|---|---|---|---|
| | λ(nm) | $\phi_P$(%)dear | $\phi_{PL}$(%)air |
| AP013 | 507 | 11.5 | 9.3 |
| AP021 | 489 | 8.0 | 7.2 |
| AP019 | 470 | 4.5 | 3.9 |
| AP022 | 471 | 2.5 | 2.0 |

[a] PMMA doped thin films (5 w/w % of compound) formed by spin-coating on a pristine quartz substrate.

Upon excitation at $\lambda_{max}$ = 360 nm the emission spectra of AP013 and AP021 display emission maxima that are much broader then slightly red shifted with respect to the parent complexes AP019 and AP022, respectively.

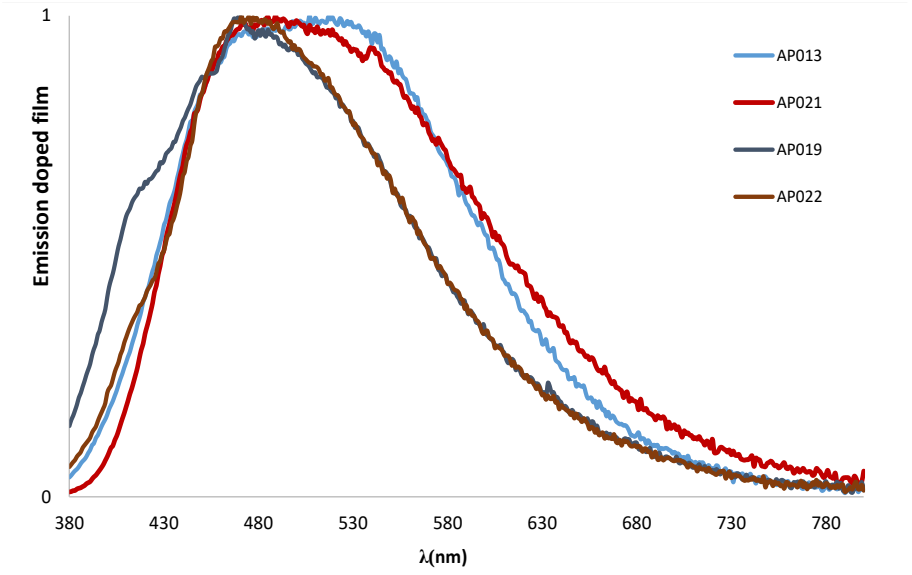


*Figure 24 Emission spectra of PMMA films in solid state*

The observed broadening of the emission profiles is typical of polymeric organic materials with electron-carrying properties. Thus, it might be supposed that the molecules packed within the PMMA matrix undergo intermolecular charge transitions π-π* among different molecules of the same species. The emission profiles of AP019 and AP022 in respect to the corresponding ligands are unstructured and present broad but not flat peaks.

The PLQY values of the free ligands and the complexes were performed in aerated and degassed conditions and obtained with an integrating sphere.

The PLQY of AP013 and AP021 were found to be very low between 11-7% in both aerated and degassed solutions.

The PLQY obtained in solid state are very different in respect to the one obtained in solution state, in fact the triplet state might be completely quenched by the π-π*stacking interactions in solid state.

The PLQY of the corresponding complexes AP019 and AP022 were found even lower than those of the corresponding free ligands (see Figure 25); the values are too close to the error limit of the performances related to the use of the integrating sphere. The occurrence of this behavior might be traced to the lack of the self aggregation effect that was recalled for explaining the emission properties of the free ligands in PMMA matrices.

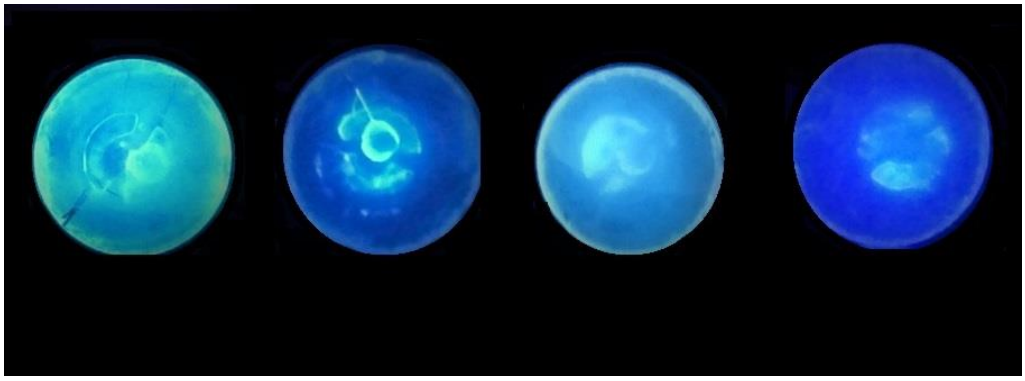

*Figure 25 PMMA films of AP013, AP019, AP021 and AP022 under UV-lamp (λexc = 365 nm).*

## *2.8 Energy gap ($\Delta E_{HOMO/LUMO}$)*

### *2.8.1 DFT calculation*

The geometrical and electronic properties of the free ligand were optimized using the Gaussian 03 programme package. Time dependent density functional theory (TD-DFT) calculations were performed on AP013 and AP021. It was used the most popular B3LYP density functional based on their ground closed shell state geometries collected by their crystal structure and optimized by DFT (B3LYP/6-31G*) method.

As shown in the Figure 26, the HOMO orbitals (bottom, Figure 26) are localised on the carbazole moiety while the LUMOs (top, Figure 26) are essentially localised on the benzophenone substituent, as expected. Actually, the phenyl ring of the benzophenone moiety seems to contribute to both HOMO and LUMO. This feature might be detrimental for the eventual TADF performances of the molecule since the design of a good TADF requires spatial separation between the coordinates of the donor (HOMO) and acceptor (LUMO) moieties. On the other hand, the overlap between HOMO and LUMO enhances the electroluminescence properties of AP013 and AP021, allowing phosphorescence to occur at room temperature in degassed solution states in respect to other D-A compound already reported in literature which show phosphorescence only in case of crystalline powder state.

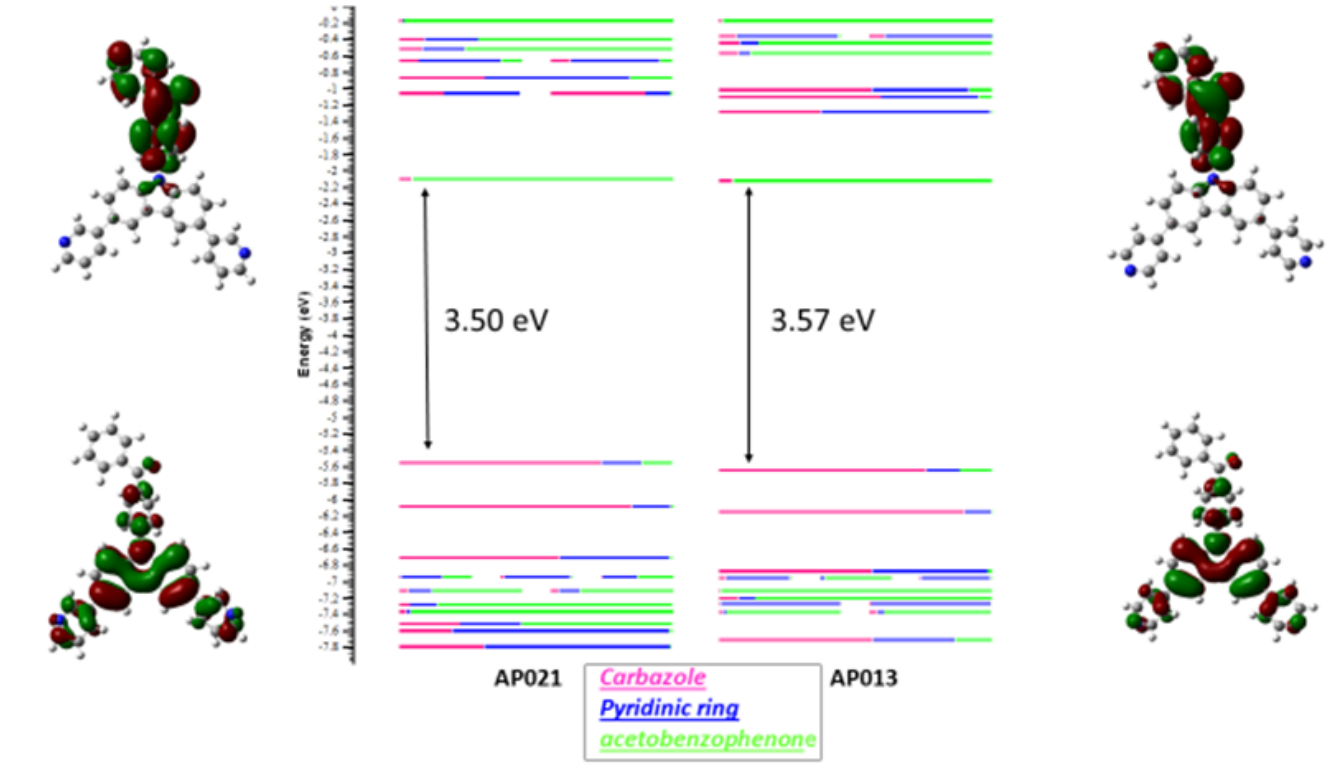


*Figure 26 DFT Calculation (S=1); approximate degenerancy of MOs energy levels threshold generancy (eV) =0.05000.*

The energy gap between the highest occupied (HOMO) and lowest unoccupied (LUMO) electronic levels is a critical parameter determing electronics, optical, redox and transport properties of a material.

In the DFT context, the calculated HOMO-LUMO gap only provides an approximation to the fundamental gap, the quality of that approximation strongly depends on the specifics of the computational methodology.[35]

For AP013 the calculated values of HOMO and LUMO were found as -5.8 and -2.23 eV, respectively, providing an energy gap of 3.57 eV.

In the case of AP021 HOMO and LUMO were calculated as -5.7 and -2.16 eV, respectively and the corresponding energy gap was 3.50 eV.

The DFT calculation were simulated in ACN, thus it is possible (approximately) to compare the data obtained with the results reported in the following paragraph dealing with the experimental evaluation of the energy of HOMO and LUMO levels by the means of cyclic voltammetry (CV) and Differential Pulse Voltammetry (DPV) of AP013 and AP021.

*2.8.2 Cyclic Voltammetry*

It is useful to mention that the solid state values of ionization potential and electron affinity are, in many instances, approximated experimentally via cyclic voltammetry measurements of the oxidation and reduction potentials carried out in solutions.

Cyclic Voltammetry (CV) and Differential Pulse Voltammetry (DPV) curves of AP013 (Figure 26) and AP021 (Figure 27) were performed in tetra-n-butylammonium hexafluorophosphate and acetonitrile solution containing 0.231mmol of the analysed compound. The CV and DPV measurements were carried out with a conventional three-electrode configuration consisting of a glassy carbon working electrode, a platinum disk auxiliary electrode and an Ag/AgCl reference electrode, and the scan speed was 0.1 V $s^{-1}$. The CV obtained were scaled using Ferrocene as a standard reference.

In order to evaluate the Energy Gap between HOMO and LUMO characterizing the synthetized ligands, *Brades*[36] empiric equation was applied

$$E\ HOMO = -Ip = (-Eox' + 4.456)eV$$

$$E\ LUMO = -Ea = (-Ered' + 4.456)eV$$

in which $Eox'$ and $Ered'$ are the onset potential values in respect to Standard Hydrogen Electrode (SHE).

The sample of AP013 showed a very different value of energy gap from what expected in respect to DFT calculation, it decreased from 3.57 to 2.28 eV.

$E_{ox\ onset/\ (SCE)}$ = 1.828 V  $E_{red\ onset/\ (SCE)}$ = -1.448 V

$E_{ox\ onset/\ (H^+/H2)} = E_{ox\ onset/\ (SCE)}$ + 0.241 V= 2.069 V

$E_{red\ onset/\ (H^+/H2)} = E_{red\ onset/\ (SCE)}$ + 0.241V= -1.207 V

$E_{HOMO}$= - ($E_{ox\ onset/\ (H^+/H2)}$ **+ 4.456) eV** = -6.525 eV

$E_{LUMO}$= - ($E_{red\ onset/\ (H^+/H2)}$ **+ 4.456) eV** = -3.249 eV

Energy gap $_{HOMO\text{-}LUMO(ox\ onset/red\ onset\ )}$= 3.28 eV

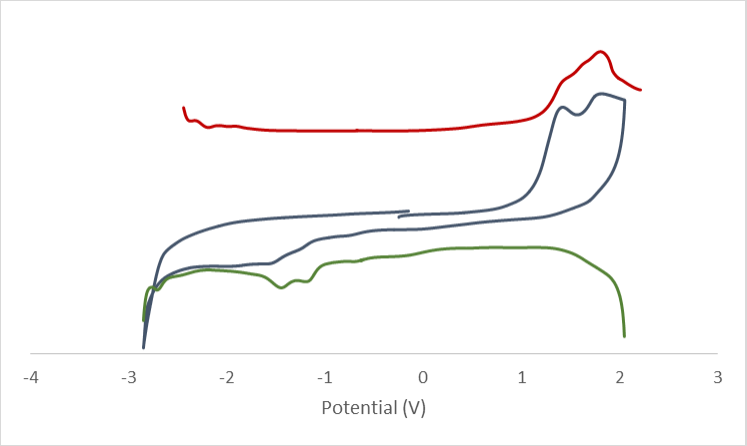


*Figure 27 AP013. Init E (V) = 0; High E (V) = 2.3; Low E (V) = -2.6; Scan Rate (V/s) = 0.1; Sample Interval (V) = 0.001; Sensitivity (A/V) = 1e-5.*

However, for AP021 the energy gap obtained is similar in respect to the one obtained by DFT calculations, 3.25 eV instead of 3.50 eV.

$E_{ox\ onset/\ (SCE)} = 1.623$ V  $E_{red\ onset/\ (SCE)} = -2.041$ V

$E_{ox\ onset/\ (H^+/H2)} = E_{ox\ onset/\ (SCE)} + 0.241$ V=1.865 V

$E_{red\ onset/\ (H^+/H2)} = E_{red\ onset/\ (SCE)} + 0.241$ V= -1.799 V

$E_{HOMO} = -(E_{ox\ onset/\ (H^+/H2)} + \mathbf{4.456})$ **eV** = -6.321 eV

$E_{LUMO} = -(E_{red\ onset/\ (H^+/H2)} + \mathbf{4.456})$ **eV** = -2.656 eV

Energy gap $_{HOMO\text{-}LUMO(ox\ onset/red\ onset\ )}$= 3.70 eV

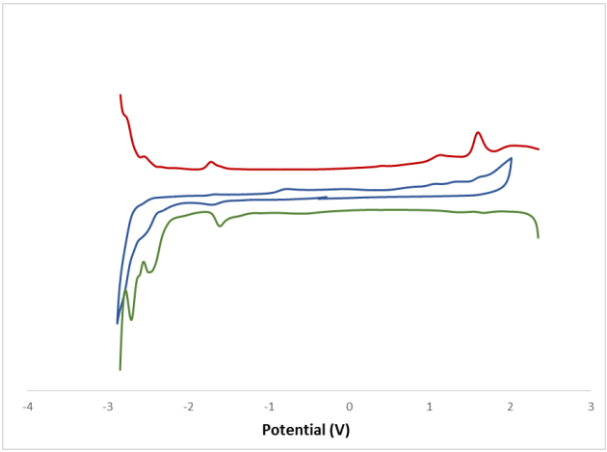


*Figure 28 Init E (V) = 0 ; High E (V) = 2.6;Low E (V) = -2.6; Scan Rate (V/s) = 0.1; Sample Interval (V) = 0.001; Sensitivity (A/V) = 1e-5.*

It is therefore possible to observe some discrepancies in the experimental data obtained with voltammetric techniques with respect to those deriving from DFT theoretical calculations. In

particular, the experimental HOMO-LUMO gaps are lower than those deduced by DFT: This difference is more pronounced in the case of AP013, enlightening a behavior that might be related to the more significant bathochromic shift of the absorption profile that is experienced by AP013 with respect to AP021 on passing from DCM to ACN.

# 3 Conclusive remarks

This experimental work was aimed to the preparation of new carbazole-type scaffolds decorated with donor and acceptor (D-A) substituents to be employed for the production of the corresponding Pd(II)-based cages. The design of the new molecules was essentially focused to the evaluation of their Thermally Activated Delayed Fluorescence (TADF) properties.

Much of the activity was dedicated to the evaluation of the synthetic strategies and procedures to attain the design of the desired donor-acceptor target compound. In particular, a bottom-up method involving the stepwise functionalization – through aromatic nucleophilic substitution (SNAr) followed by Suzuki coupling - of the starting 3,6-dibromo-9H-carbazole was developed. Once the initial step was optimized, the carbazole-based compound was submitted to Suzuki reactions in order to obtain molecules in which the 4-pyridyl (AP013) or 3-pyridyl (AP021) rings were appended to the carbazole core units.

Then, complexation of both the ligands AP013 an AP021 with Pd(II) leads to the formation of different Pd(II)-based cages. The characterization of the cages involved the use of Nuclear Magnetic techniques such as DOSY and $^{1}$H-NMR.

All of the desired products showed optoelectronic properties. Absorption and emission spectroscopy was used to evaluate the electroluminescence properties and to characterize the different compounds. Moreover, PLQY and lifetime decays values were also included into the final work in accordance to the estimation of TADF characteristics studies.

However, as far as we can evince from this studies, the sole AP013 might be classified as a promising compound to achieve TAD Fluorescence.

Furthermore, the magnitude of the HOMO LUMO gap was estimated by theoretical DFT calculations and the results were compared obtained by voltammetric techniques such as cyclic voltammetry (CV) and differential pulse voltammetry (DPV).

# 4 Experimental Part

## *4.1 General Synthetic Procedures*

Commercial chemicals were used as supplied. All reactions were performed using standard Schlenk techniques under inert ($N_2$) atmosphere with reagent-grade solvents. Flash column chromatography was performed using silica gel (Silia-P from Silicycle, 60 Å, 40-63 µm). Analytical thin layer chromatography (TLC) was performed with silica plates with aluminum backings (250 µm with indicator F-254). Compounds were visualized under UV light. $^1$H and solution-phase NMR spectra were recorded on a Bruker Avance spectrometer operating at 11.7 T (Bruker AVIIIHD, AVIII and AV 700,500 and 400 MHz, respectively). The following abbreviations have been used for multiplicity assignments: “s” for singlet, “d” for doublet, “dd” double doublet,“t” for triplet, “m” for multiplet and “br” for broad. $^1$H NMR spectra were referenced to the solvent peak. Melting points (Mps) were recorded using open-ended capillaries on an electrothermal melting point apparatus and are uncorrected. High-resolution mass spectra were recorded at the EPSRC UK National Mass Spectrometry Facility at Swansea University on a quadrupole time-of-flight (ESI-Q-TOF), model ABSciex 5600 Triple TOF in positive electrospray ionization mode and spectra were recorded using sodium formate solution as the calibrant.

## *4.2 Photophysical data*

All samples were prepared in HPLC grade dichloromethane and acetonitrile. Absorption spectra were recorded at room temperature using a Shimadzu UV-1800 double beam spectrophotometer. Molar absorptivity determination was verified by linear least-squares fit of values obtained from at least four independent solutions at varying concentrations ranging from $4.41 \times 10^{-4}$ to $5.09 \times 10^{-5}$ M. The sample solutions for the emission spectra were prepared in HPLC grade dichloromethane and acetonitrile, degassed via three freeze−pump−thaw cycles using a quartz cuvette. Steady-state and time-resolved emission spectra were recorded at 298 K using Edinburgh Instruments F980 Fluorimeter. All samples for steady-state measurements were excited at 360 nm. The excited-state lifetimes of the samples were obtained by time correlated single photon counting (TCSPC) at an excitation wavelength of 360 nm using an Edinburgh Instruments F980 fluorimeter using a pulsed diode laser, and PL emission was detected at the corresponding steady-state emission maximum for each sample. Emission quantum yields were determined using the optically dilute method. A stock solution with absorbance of ca. 1.360 was prepared, and then four dilutions were prepared with absorbances of ca. 0.1088, 0.0742, 0.0551, 0.0276 respectively. The Beer−Lambert law was found to be linear at the concentrations of the solutions. The emission spectra were then measured after the solutions were degassed by nitrogen purging for fifteen minutes per sample prior to spectrum acquisition. For each sample, linearity between absorption and emission intensity was verified through linear regression analysis. Individual relative quantum yield values were calculated for each solution, and the values reported represent the slope value. The $\phi_s = \phi_r(A_r/A_s)(I_s/I_r)(n_s/n_r)_2$ equation was used to calculate the relative quantum yield of each of the sample, where $\phi_r$ is the absolute quantum yield of the reference, *n* is the refractive index of the solvent, A is the absorbace at the excitation wavelength, and I is the integrated area under the corrected emission curve. The subscripts s and r refer to the sample and reference, respectively. A solution of quinine sulphate in 0.5M $H_2SO_4$ was used as a reference.

*4.3 Synthesis of 3,6-dibromo-9H-carbazole*

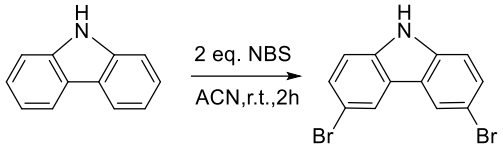


To a 0°C solution of 9H-carbazole (5gr, 0.03 mol, 1 equiv.) dissolved in a round bottomed flask in ACN (10 mL) a solution of NBS (10.68 g, 0.06 mol, 2 equiv.) in 40 mL ACN was added via addition funnel. The solution was allowed to come to room temperature (r.t.) and stirred for an additional period of 2 hours. The reaction was quenched with $H_2O$, ethyl acetate was added and the layers separated. The aqueous phase was dried over $MgSO_4$, the organic phase was concentrated under reduced pressure then under vacuum. A green powder was obtained.

**Yield**: 87%.

**$^1$H NMR** (500 MHz, Chloroform-*d*) δ ppm 8.16 (d, *J* = 2.0 Hz, 2H, 7.55 (dd, $J_{ortho}$ 8.6; $J_{meta}$ 1.9 Hz, 2H), 7.34 (d, *J* = 8.6 Hz, 2H).

*4.4 Synthesis of (4-(3,6-dibromo-9H-carbazol-9-yl)phenyl)(phenyl)methanone*

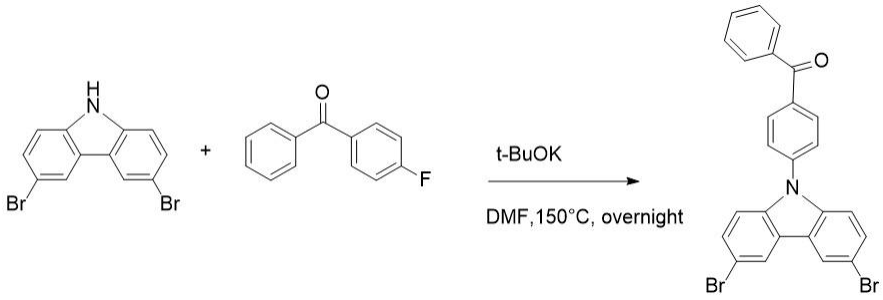


3,6-dibromocarbazole (1.5 g, 4.61 mmol, 1 equiv.) and potassium tert-butoxide (0.52 g, 4.61 mmol, 1 equiv.) were dissolved in a flask fitted with a magnetic stirrer and condenser in dry DMF (25 mL). The mixture was heat at 150 °C for 30 min and then 4-Fluorobenzofenone (0.92 g, 4.61 mmol, 1 equiv.) was added for overnight. The reaction mixture was cooled down and poured in ice-water. The organic phase was extracted with DCM. The organic phase was concentrated under reduced pressure under vacuum. The product was recrystallized from EtOH. A white powder was collected.

**Yield**:44%.

**$R_f$**: 0.76 in DCM.

**Melting Point**: 226-228°C.

**$^1$H NMR** (500 MHz, Chloroform-d) δ ppm 8.26 – 8.22 (d, 2H), 8.12 – 8.08 (m, 2H), 7.95 – 7.90 (dd, 2H), 7.71 – 7.65 (m, 3H), 7.60 – 7.55 (m, 4H), 7.39 (d, J = 8.7Hz, 2H).

**$^{13}$C NMR** (500 MHz, Chloroform-d) δ ppm 195.45, 140.57, 139.29, 137.18, 136.73, 132.85, 132.06, 129.68, 128.53, 126.26, 124.38, 123.42, 113.71, 111.50.

**HR-MS** $C_{25}H_{15}Br_2NO$ theoretical isotope model m/z: 505. 9573 observed m/z: 505.9565.

*4.5 Synthesis of*

*(4-(3,6-di(pyridin-4-yl)-9H-carbazol-9-yl)phenyl)(phenyl)methanone*

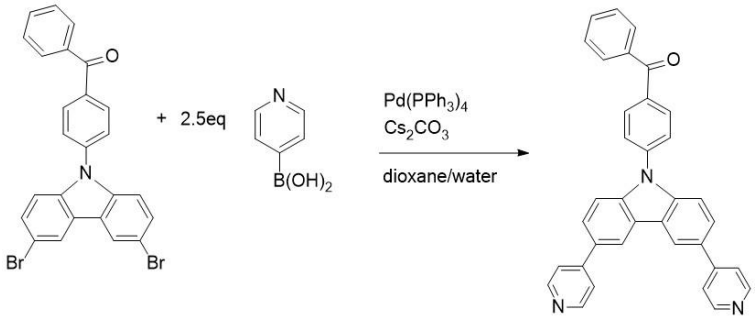


In a 250mL round bottomed flask a solution of (4-(3,6-dibromo-9H-carbazol-9-yl)phenyl)(phenyl)methanone (0.400g, 0.792 mmol,1 equiv.) is dissolved in a mixture of 30 mL 1,4-dioxane and degassed water (2:1). Then 4-Pyridinylboronic acid (0.245 g, 1.99 mmol, 2.5 equiv.), $Cs_2CO_3$ (1.55 g, 4.75 mmol, 6 equiv.) and $Pd(PPh_3)_4$ (0.091 g, 0.0792 mol, 600% mol) were successively added under nitrogen. The solution was refluxed at 105°C for 72 h. After cooling to r.t., $H_2O$ (10 mL) and brine (10 mL) were added. The mixture was extracted with DCM 50 mL. After drying ($MgSO_4$) and evaporation of the solvent, the residue was purified by flash column chromatography (silica gel column, 3:1 $CH_2Cl_2$/Hexane 40% $Et_3N$).

A yellow powder was obtained.

**Yield**: 55.4%.

**Rf** = 0.54 in 3:1 $CH_2Cl_2$/Hexane 40% Et3N.

**Melting Point**: 200-202°C.

**$^1$H NMR** (500 MHz, Chloroform-d) δ ppm 8.74 – 8.70 (dd, 4H), 8.55 – 8.52 (d, 2H), 8.16 – 8.13 (m, 2H), 7.98 – 7.93 (dd, 2H), 7.82 – 7.77 (m, 4H), 7.72 – 7.68 (m, 4H),7.68-7.67 (t,1H),7.67-7.64 (m,2H), 7.62 – 7.57 (m, 2H).

**DOSY** (ns 16, D20 0.1, P30 1800) D($m^2$/s)=1.7e-10.

**$^{13}$C NMR** (500MHz, CDCl3) δ ppm 195.52, 150.25, 148.64, 141.30, 140.77, 137.20, 136.77, 132.88, 132.09, 131.17, 130.09, 128.56, 126.33, 125.84, 124.39, 121.72, 119.23, 110.79.

**HR-MS** $C_{35}H_{24}N_3O$ theoretical isotope model m/z: 502.1914 observed m/z: 502.1902.

## *4.6 Synthesis of*

## *(4-(3,6-di(pyridin-3-yl)-9H-carbazol-9-yl)phenyl)(phenyl)methanone*

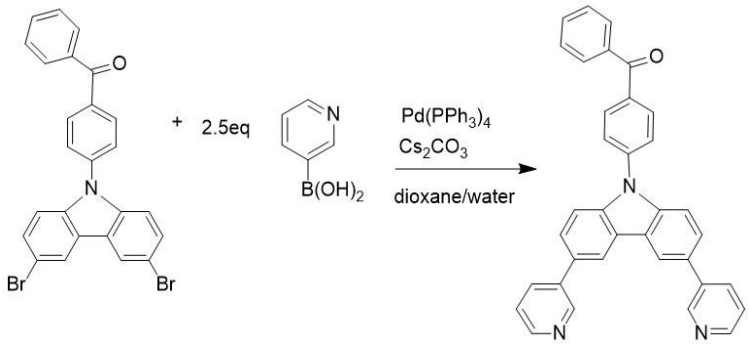


In a 250mL round bottomed flask a solution of (4-(3,6-dibromo-9H-carbazol-9-yl)phenyl)(phenyl)methanone (0.400 g, 0.792 mmol, 1 equiv.) is dissolved in a mixture of 30 mL 1,4-dioxane and degassed water (2:1). Then 3-Pyridinylboronic acid (0.245 g, 1.99 mmol, 2.5 equiv.), $Cs_2CO_3$ (1.55 g, 4.75 mmol, 6 equiv.) and $Pd(PPh_3)_4$ (0.091 g, 0.0792 mol, 600% mol) were successively added under nitrogen. The solution was refluxed at 105°C for 72 h. After cooling to r.t., $H_2O$ (10 mL) and brine (10 mL) were added. The mixture was extracted with DCM 50 mL. After drying ($MgSO_4$) and evaporation of the solvent, the residue was purified by flash column chromatography (silica gel column, 3:1 $CH_2Cl_2$/Hexane 40% $Et_3N$). A yellow powder was obtained.

**Yield**: 55.4%.

**Rf** = 0.50 in 3:1 $CH_2Cl_2$/Hexane 40% $Et_3N$.

**Melting Point**199-200°C.

**$^1$H NMR** (500 MHz, Chloroform-d) δ ppm 9.03 – 9.01 (dd, 2H), 8.66-8.64(dd, J = 4.8, 1.6 Hz, 2H), 8.44 (d, J = 1.6 Hz, 2H), 8.17-8.14 (m, J = 8.4 Hz, 2H), 8.07 – 8.04 (m, 2H), 7.97 – 7.94 (m, 2H), 7.83-7.79 (m, J = 8.4 Hz, 2H), 7.75-7.72 (dd, J = 8.6, 1.8 Hz, 2H), 7.69 – 7.65 (m, 3H), 7.62-7.57 (m, J = 7.6 Hz, 2H), 7.69-7.65 (m, 3H), 7.46 – 7.43 (dd, 2H).

**$^{13}$C NMR** (126 MHz, $CDCl_3$) δ ppm 207.07, 148.48, 148.06, 140.62, 137.28, 137.05, 134.50, 132.82, 132.07, 130.92, 130.08, 128.53, 126.29, 125.99, 124.43, 123.66, 119.24, 110.73.

**HR-MS** $C_{35}H_{24}N_3O$ theoretical isotope model m/z: 502.1914 observed m/z: 502.1902.

## *4.7 Synthesis of 3,6-dibromo-9-phenyl-9H-carbazole*

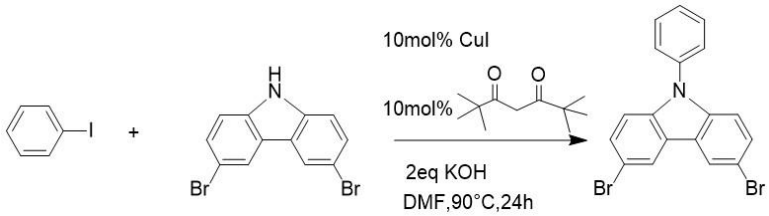


In a 50 mL shlenck a mixture of 3,6-dibromo-9H-carbazole (1.35mmol, 0.438 g), aryl iodide (2.70 mmol, 0.3 mL), 2,2,6,6-tetramethylheptane-3,5-dione (0.135 mmol, 0.03 mL) and anhydrous KOH (2.70 mmol, 0.150 g) were dissolved in 10mL of dry DMF. An amount of CuI 10%mmol (0.135mmol, 0.026 g) was added to the mixture after it was degassed and stirred under nitrogen atmosphere.
The reaction mixture was heat to 130°C and it was allowed to react for 24 hours under nitrogen.
After cooling down the mixture was quenched with brine and the organic phase was separated with DCM (3x15mL). The product was isolated by flash column chromatography (silica gel column, 2:1 $CH_2Cl_2$/hexane).
A white powder was obtained .
**Yield**: 37%.
**Rf** = 0.92 in 2:1 $CH_2Cl_2$/Hexane.
**Melting Point** 164-166°C.
**$^1$H NMR** (500 MHz, Chloroform-d) δ ppm 8.22 (d, J = 1.8 Hz, 2H), 7.68 – 7.61 (m, 2H), 7.56 – 7.50 (m, 5H), 7.28 (d, J = 8.3 Hz, 2H).
**$^{13}$C NMR** (126 MHz, CDCl3) δ ppm139.87, 136.78, 130.13, 129.38, 128.12, 126.97, 123.92, 123.21, 113.04, 111.52.

## *4.8 Synthesis of supramolecular cage with $Pd^{2+}$ and (4-(3,6-di(pyridin-4-yl)-9H-carbazol-9-yl)phenyl)(phenyl)methanone*


(4-(3,6-di(pyridin-4-yl)-9H-carbazol-9-yl)phenyl)(phenyl)methanone (0.010g ,1.99 $10^{-2}$ mmol, 1 equiv.) was dissolved in 3mL DMSO-d6 and degassed under nitrogen atmosphere in a 5 mL vial. Then $[Pd(CH_3CN)_4BF_4]^{2-}$ (0.022g ,4.98 $10^{-2}$mmol, 2.5 equiv.) was added to the degassed solution under nitrogen atmosphere and the reaction was allowed to react for 2 days at 80°C.

The reaction mixture was cooled at room temperature and the solid was obtained by precipitation with iced water. The solid was washed with a solution of hexane/diethyl ether 1:1.

**Melting point**: 159-160°C.

**$^1$H NMR** (500 MHz, DMSO) δ ppm 9.10, 9.01, 8.85, 8.41, 8.11-8.00, 7.90-7.85,7.75-7.70,7.60-7.58.

**DOSY** (n.s.16, D2O 0.6, P30 800) D ($m^2$/s) = 1.9 x $10^{-11}$

*4.9 Synthesis of supramolecular cage with $Pd^{2+}$ and (4-(3,6-di(pyridin-3-yl)-9H-carbazol-9-yl)phenyl)(phenyl)methanone*

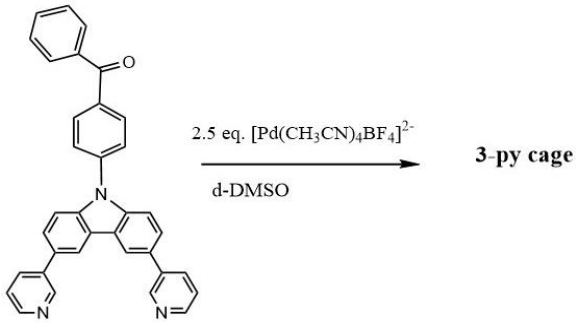


(4-(3,6-di(pyridin-3-yl)-9H-carbazol-9-yl)phenyl)(phenyl)methanone (0.010g, 1.99 $10^{-2}$ mmol,1 equiv.) was dissolved in 3mL DMSO-d6 and degassed under nitrogen atmosphere in a 5 mL vial. Then $[Pd(CH_3CN)_4BF_4]^{2-}$ (0.022g, 4.98 $10^{-2}$ mmol, 2.5 equiv.) was added to the degassed solution under nitrogen atmosphere and the reaction was allowed to react for 2 days at 80°C.The reaction mixture was cooled at room temperature and the solid was obtained by precipitation with iced water. The solid was washed with a solution of hexane/diethyl ether 1:1.

**Melting point**: 152-154°C.

**$^1$H NMR** (500 MHz, DMSO) δ ppm 9.21, 8.89, 8.71, 8.47- 8.46, 7.95-7.91, 7.89-7.84, 7.84, 7.75-7.50.

# Bibliography


[1] C. Adachi, M.A. Baldo, M.E. Thompson, S.R. Forrest, J. Appl. Phys., 2010, 90, 5048-5051

[2] D.Y. Kondakov, T.D. Pawlich, T.K. Hatwar, J.P. Spindler, J. Appl. Phys, 2009, 106, 124510-124518

[3] Paola Ceroni,Chem1, 2016, 522-530, Elsevier

[4] Chihaya Adachi, Japanese Journal of Applied Physics, 2014, 53, Comprehensive Review

[5] M. Yoshizawa, S. Miyagi, M. Kawano, K. Ishiguro, Makoto Fujita, JACS, 2004, 126, 9169-9173

[6] T. Hiroki, M. Takashi, G. Resnati, P. Metrangolo, M. Fujita, Angew. Chem. Int. Ed., 2015, 54, 8411-8414

[7] Quing Fu Sun, Junji Iwasa, Daichi Ogawa, Yoshitaka Ishido, Sota Sato, Makoto Fujita, 2010, Science, 328, 1144-1148

[8] Elliott Anastasia , Lewis James, Van Der Salm Holly, McAdam C. John, Crowley James D., Gordon Keith C., Inorganic Chemistry,2016, 55, 3440-3447

[9] http://www.cope.gatech.edu/?q=august-23-2013-dr-chihaya-adachi

[10] Carlos Baleizao and Mario Berneran-Santos, The Journal of Chemical Physics, 2007, 126

[11] Uoyama Hiroki,Goushi Kenichi, Shizu Katsuyuki,Nomura Hiroko,Adachi Chihaya, Nature, 2012, 492, 234-238

[12] D. Beljonne, Z. Shuai, G.Pourtois, and J.L. Bredas, J.Phys. Chem, 2001, 105, 3899-3907

[13] Bin Hu, Yujian Zhang, Mi Ouyang, Zhiyan Fu, Chend Zhang, Journal of Electroanalytical Chemistry, 2013, 689, 291-296

[14] The Great Soviet Encyclopedia, 3rd Edition (1970-1979). © 2010

[15] Daniel C.Harris, Chimica Analitica Quantitativa, 2005, 407-405

[16] F. Puntoriero, F. Nastasi, M. Galletta, S.Campagna, Comprehensive Inorganic Chemistry II, 2013, 255-337

[17] Markus J. Leitl, Daniel M. Zink, Alexander Schinabeck, Thomas Baumann, Daniel Volz, Hartmut Yersin, Top Curr. Chem., 2016, Review

[18] Vincenzo Balzani, Giacomo Bergamini, Paola Ceroni, Angew. Chem. Int. Ed., 2015, 54, 2-20

[19] Ju Sik Kang, Tae Ryang Hong, Hyung Jong Kim, Young Hoon Son et al., Journal of Materials Chemistry C, 2016,4, 4512-4520

[20] http://www.uniregensburg.de/Fakultaeten/nat_Fak_IV/Physikalische_Chemie/Yersin/SiHa.pdf

[21] David,Grave,Richard(2015), Durham Thesis, Durham University, Thesis avaible on line: http://ettheses.dur.ac.uk/11255 20/02/2017

[22] Sun Qing-fu,Sato Sota,Fujita Makoto, Angew. Chem. Int. Ed, 2014, 12, 2-6

[23] Fujita Makoto, Aoyagi Masaru,Ogura Katsuyuki, Inorganica Chimica Acta, 1996,246, 53-57

[24] D. Fujita, H. Yokoyama, Y. Ueda, S.Sato, M, Fujita, Angew. Chem. Int. Ed, 2015, 54, 155-158

[25] D. K.Chand, K. Biradha, M. Fujita, Chem. Comm., 2002, 2, 2486-2489

[26] Yongyang Gong, Gan Chen, Quian Peng, Wang Zhang Yuan, Ben Zhong Tang, Advanced Materials,2015, 27, 6195-6201

[27] Hu Bin, Lv Xiaojing, Sun Jingwei, Bian Gaofeng ,Ouyang Mi ,Fu Zhiyan, Organic Electronics, 2013, 14, 1521-1530

[28] Rembiak Andreas, Koskinen Ari M P, Synthesis, 2015,47, 3347-3353

[29] Zysman-Colman Eli ,Arias Karla ,Siegel Jay S, Can. J. Chem., 2009, 87, 440–447

[30] Fei Chen, Ning Liu, Enhui Ji and Bin Dai, RSC ADv., 2015, 5, 51512-51523

[31] D. Fujita, H. Yokoyama, Y. Ueda, S. Sato, 2015, Angew. Chem.Int. Ed. ,16, 155-158

[32] Smulders Maarten M. J., Riddell Imogen, Browne Colm ,Nitschke Jonathan R., Chemical Society Reviews, 2013, 1728-1754

[33] M.Fujita, K.Ogura, Coordination Chemistry Review, 1996, 148, 249-269

[34] S. Dipak, S. Partha, Chem. Eur. J., 2014, 20, 12483- 12492

[35] Jean-Luc Bredas, Mater. Horiz, 2014, 1, 17-19

[36] C.M. Cardona, W. Li, A. E. Kaifer, G. C. Bazan, Adv. Mater., 2011, 23,2367-2371